TECHNIQUES FOR STOCHASTIC SIMULATION OF COMPLEX ELECTROMAGNETIC AND CIRCUIT SYSTEMS WITH UNCERTAINTIES

BY

XU CHEN

DISSERTATION

Submitted in partial fulfillment of the requirements
for the degree of Doctor of Philosophy in Electrical and Computer Engineering
in the Graduate College of the
University of Illinois at Urbana-Champaign, 2018

Urbana, Illinois

Doctoral Committee:

Professor Andreas C. Cangellaris, Chair
Professor José E. Schutt-Ainé
Professor Tamer Başar
Professor Umberto Ravaioli

ABSTRACT

This thesis presents a set of tools and methodologies that perform fast stochastic characterization and simulation of uncertainties in electromagnetic and circuit systems. Background information on polynomial chaos and fast stochastic numerical techniques is reviewed, and discussion is offered on comparison of different approaches to stochastic simulations. The formulation for Stochastic LIM, a Stochastic Galerkin Method-based time-domain circuit solver, is presented, and some simulation results are shown comparing the new solver to Monte Carlo techniques using a commercial circuit solver. The simulator is then used to simulate several transmission line problems, including single- and multi-conductor, crosstalk, and coupled-line on a printed circuit board substrate with fiber-weave effect. Stochastic Collocation technique is discussed as a method to characterize multi-level electromagnetic-circuit simulations. A method to use Monte Carlo integration to evaluate interpolation residual is presented. The effectiveness of the proposed method is demonstrated with a high-order problem of electromagnetic waves causing interference on a printed circuit board inside a vehicle with apertures. The effectiveness of the multi-level analysis methodology is demonstrated using eye diagram opening as cost function. Additionally, a wavelet-based Stochastic Collocation technique is introduced to solve circuit problems with resonant behavior. Finally, we discuss the overall work presented in this thesis and discuss several future research directions to extend the results presented here.

To my teachers, and their teachers.

ACKNOWLEDGMENTS

This thesis marks the conclusion of a long and fruitful journey in my life. In addition to the technical discoveries presented in this document, I have also made numerous discoveries regarding myself and the value of all the people in my life. This thesis would not be complete without a discussion of the contributions of said people.

First, all the discoveries presented in this thesis would not exist without the trust and generosity from my advisors, Prof. Andreas Cangellaris and Prof. Jose Schutt-Aine. I am forever grateful to them for giving me the opportunity to collaborate with them, for working tirelessly to provide support for my research, for carving time out of their busy schedules, and for caring about me. Their efforts have taught me the value of good teachers and mentors. I can only hope to one day pass this favor on.

My dissertation committee members have offered invaluable advice throughout the thesis-writing process. Hence I would like to thank Prof. Tamer Basar and Prof. Umberto Ravaioli for their time and effort spent to serve on my committee. I have also taken very well-taught courses from these individuals during my education, and they have not only helped me master many technical topics, but have also demonstrated to me the characteristics of great teachers.

I discovered the value of a strong professional network during the course of my studies. Many of these people are also my teachers and mentors, and their support was essential to my professional development. In this regard, I would like to acknowledge all my professional colleagues, especially Dr. Dale Becker at IBM, Tom Savarino at Apple, George Katopis, Dr. Wendem Beyene, Dr. Aosheng Rong, and in particular Glen Salo, whom I had the joy of collaborating with over the last few years. I look forward to collaborating with these individuals and many others in the

future.

Many faculty members at the University of Illinois have offered me advice and mentorship during my teaching assistantships and teaching experiences. These people are my teachers and mentors for my role as an educator. The incomplete list includes Prof. Lara Waldrop, Prof. Lynford Goddard, Prof. Peter Dragic, Prof. Dan Wasserman, Prof. Wei He, Prof. Arne Fliflet, Prof. Songbin Gong, Prof. Patricia Franke, and Prof. Zhi-Pei Liang. I have learned a great deal by observing these individuals perform their teaching duties with the utmost care and professionalism. In particular, I must acknowledge Prof. Erhan Kudeki for giving me the opportunity to teach.

Another discovery resulting from the work of this thesis is the value of friends and colleagues around the office. To this end, I would like to acknowledge all the past and present members of the Electromagnetics Lab. In particular, I have benefitted a great deal from being around Dr. Juan Ochoa, Dr. Tom Comberiate, Dr. Tian-Jian Lu, Xiao Ma, Thong Nguyen, Rishi Ratan, Gene Shiue, Da Wei, Dr. Jian Guan, Dr. Kedi Zhang, and many others.

I am also happy to report that teaching others is indeed the best way to learn. I would like to acknowledge all of my past students from ECE 329, as well as the following brave individuals who volunteered to have me advise their undergraduate research: Tong Zhang, Michael Qiu, Nancy Zhao, Xiou Ge, Paprapee Buason, Diyu Yang, Yijia Xu, Elizabeth Roels, Joshua Choo, Shivani Iyer, Alan Yang, and Alaa Qarooni. Facts suggest that I have scared at least one of them off, but statistically they are much more likely to stay than the average undergraduate student.

The greatest discovery resulting from the writing of this thesis is undoubtedly that my family loves me, and that my time spent with them is the more important half of my life. Hence I would like to thank the following individuals without salutations: Yuting Chen, Victor Chen, Zhaoqing Chen, Wynter Chen. Thank you for the unconditional trust and patience that you have given me because of love. Without you, I probably would have given up on myself a long time ago. Fortunately, we will never know that for sure.

TABLE OF CONTENTS

LIST OF TABLES viii

LIST OF FIGURES ix

CHAPTER 1 INTRODUCTION 1
1.1 Motivation 1
1.2 Outline 2

CHAPTER 2 BACKGROUND 4
2.1 Polynomial Chaos 4
2.2 Non-Sampling Approaches 7
2.3 Sampling Approaches 9
2.4 Dimensionality Reduction 12
2.5 Adaptive Mesh Refinement 13

CHAPTER 3 STOCHASTIC LIM 16
3.1 Introduction 16
3.2 Deterministic LIM 18
3.3 Stochastic Galerkin Method Approach 19
3.4 Stochastic Collocation Approach 25
3.5 Stability Conditions 29
3.6 Conclusions 31

CHAPTER 4 SIMULATION OF TRANSMISSION LINES WITH UNCERTAINTIES 33
4.1 Sampling-based EM Extraction 33
4.2 Lumped Transmission Line Model 36
4.3 Numerical Examples 39
4.4 Benchmark and Conclusions 51

CHAPTER 5 STOCHASTIC SIMULATION OF MULTI-LEVEL AND RESONANT SYSTEMS 56
5.1 Non-intrusive Stochastic Collocation Approach 56
5.2 Multi-level EM and Circuit Simulation 58
5.3 Monte Carlo Evaluation of Interpolation Residual 62
5.4 Numerical Example: RF Box in Vehicle 64
5.5 Adaptive Stochastic Collocation Using Wavelet Basis 72
5.6 Numerical Example: RLC Resonator Circuit 75
5.7 Conclusions 80

CHAPTER 6 DISCUSSION AND FUTURE RESEARCH 81
6.1 Discussion 81
6.2 Future Research 82

REFERENCES 86

LIST OF TABLES

2.1 Hermite polynomials ψ_k for expansion of 4 random dimensions with order $p = 2$. [13] 5
2.2 Legendre polynomials ϕ_k for expansion of 1 random dimension with order $p = 5$. 7

4.1 Random parameters for single microstrip line with geometric uncertainties. 40
4.2 Random parameters for coupled microstrip line with geometric uncertainties. 44
4.3 Computational time comparison of Stochastic LIM implemented in MATLAB vs. Monte Carlo $N = 1000$ with Ansys Nexxim using W-element model. Parallel computing is used for Monte Carlo and EM simulations. 53
4.4 Computational time comparison of Stochastic LIM compiled using C++ vs. Monte Carlo $N = 1000$ simulation with Ansys Nexxim lumped circuit model. Parallel computing over 3 cores is used for Monte Carlo and EM simulations. 53
4.5 Data storage and post-processing requirements for coupled line and fiber-weave examples. Monte Carlo results correspond to $N = 1000$ runs using Ansys Nexxim. 55

5.1 Number of sparse grid nodes for $d = \{2, 6\}$ and $k = \{1, \ldots, 7\}$. 59

LIST OF FIGURES

2.1 Sparse grid vs. full tensor-product grid for $d = 2$ case and $k = 5$. The one-dimensional rules of both grids are equivalent, but the sparse grid has 145 nodes whereas the full tensor product grid requires 1089 nodes. [20] 11
2.2 Nesting structure of $d = 2$ Smolyak sparse grids. Levels $k = \{4, 5, 6\}$ are shown. 13
2.3 Example of an anisotropically refined sparse grid. 14
2.4 Example of a locally refined sparse grid. 15

3.1 Node and branch topology for Latency Insertion Method. 19
3.2 Circuit diagram of resistor network used in example. The element values are: $R_{12} = 14.53\Omega, R_{13} = 4.53\Omega, R_{14} = 5.3\Omega, R_{23} = 25.3\Omega, R_{24} = 47.3\Omega, L_{12} = 32.4\text{nH}, L_{13} = 22\text{nH}, L_{14} = 32.2\text{nH}, L_{23} = 32.2\text{nH}, L_{24} = 43.2\text{nH}, C_1 = 10\text{pF}, C_2 = 20\text{pF}, C_3 = 20\text{pF}, C_4 = 0.2\text{pF}$. The resistors to ground are Gaussian random variables: $R_1(\omega) = (50 + 5\xi_1)\Omega, R_2(\omega) = (10 + 1\xi_2)\text{M}\Omega, R_3(\omega) = (10 + 1\xi_3)\text{M}\Omega, R_4(\omega) = (50 + 5\xi_4)\Omega$. 26
3.3 Stochastic LIM vs. Monte Carlo results for example shown in Figure 3.2 with scaling factor $s = 1$. The mean and standard deviation show excellent agreement. 27
3.4 Stochastic LIM vs. Monte Carlo results for example shown in Figure 3.2 with scaling factor $s = 0.1$. With low latencies, the circuit is almost entirely resistive. 28
3.5 Workflow for Stochastic Collocation approach to random simulations with LIM. 30

4.1 Lumped single-line transmission line circuit in $\pi-$topology. 36
4.2 Lumped $\pi-$model for coupled transmission line. 37

4.3 Cross-section of the single microstrip line model. The random parameters in this model are dielectric constant ϵ_r, substrate thickness h, and line width W, each with an independent Gaussian distribution. 39
4.4 The excitation function V_{in}. For this simulation, $t_d = 1$ ns, $t_r = 500$ ps, $pw = 20$ ns. 40
4.5 Simulation setup for single-line pulse excitation simulation over microstrip line. 41
4.6 Voltages at near-end and far-end of single-line microstrip with geometric and material uncertainties. Shaded region represents the mean response $\pm 3\sigma$ as calculated by Stochastic LIM. The solid lines represent 21 deterministic simulations using Ansys Nexxim simulator. 42
4.7 Standard deviation σ of near- and far-end voltage on single-line microstrip with geometric uncertainties as calculated by Monte Carlo $N = 2000$ and Stochastic LIM. 43
4.8 Cross-section of coupled microstrip line. The random parameters in this model are substrate dielectric constant ϵ_r, substrate thickness h, and edge-to-edge spacing s, each with an independent Gaussian distribution. 44
4.9 Simulation setup for crosstalk simulation over coupled microstrip line. 45
4.10 Near-end crosstalk (NEXT) results of coupled transmission line simulation. Shaded region represents the mean response $\pm 3\sigma$ as calculated by Stochastic LIM. The solid lines represent 21 deterministic simulations using Ansys Nexxim simulator. 46
4.11 Standard deviation σ of NEXT as calculated by Monte Carlo $N = 2000$ and Stochastic LIM. 47
4.12 Far-end crosstalk results of coupled transmission line simulation. Shaded region represents the mean response $\pm 3\sigma$ as calculated by Stochastic LIM. The solid lines represent 21 deterministic simulations using Ansys Nexxim simulator. 48
4.13 Standard deviation σ of FEXT as calculated by Monte Carlo $N = 2000$ and Stochastic LIM. 49
4.14 Cross-section of coupled microstrip line with fiber bundles. 50
4.15 Differential signal simulation setup. The signals V_p and V_n are complementary clock signals operating at 2 Gbps, with $t_r = t_f = 200$ ps. 51

4.16 Differential voltage measured at the input and output of the coupled transmission line. The shaded areas represent mean voltage $\pm 2\sigma$ as calculated by Stochastic LIM. The black lines represent deterministic solutions calculated using ANSYS Nexxim. 52

5.1 Workflow of multi-level and multi-scale EM/circuit stochastic simulation using SC. 60
5.2 Vehicle with RF box situated inside at a fixed location. The height of the front aperture $t_1 \sim \mathcal{U}(0.2,\, 0.6)$ (m) and the width of the rear aperture $w_2 \sim \mathcal{U}(0.2,\, 1.0)$ (m) are random variables. 61
5.3 Interpolation $\tilde{f}(\vec{x}) = |V_{noise1}|$ for (a) $k = 3$ and (b) $k = 7$. The points shown are interpolation nodes. 65
5.4 Residual calculated at sparse grid nodes and Monte Carlo points for $k = 3$ and $k = 6$. 66
5.5 Convergence of L_2 norm of residual over the random space. 67
5.6 Circuit for simulating eye diagram of 5 Gbps signal with RF interference. 69
5.7 Eye diagram of the voltage seen at receiver input. The measured eye width is shown at upper right corner of the plot. 69
5.8 Response surface of eye width in random space. 70
5.9 Response surface of noise voltage source 1 and noise voltage source 2. 71
5.10 PDF of eye width calculated using SC and MC. 72
5.11 Flowchart of the Adaptive Wavelet Stochastic Collocation Method, with feedback adaptive refinement. 76
5.12 Lossless transmission line terminated by an RLC circuit, showing parameters used in 2D interpolation. 76
5.13 Approximated $Re\{V_c\}$ and $Im\{V_c\}$ using approx. 1000 points and adaptive grid used to approximate $Re\{V_c\}$ with 967 points. 78
5.14 Residual (log scale) vs. grid size for wavelet, linear piecewise polynomials, and non-adaptive global grids for two and four random parameters. 79

CHAPTER 1

INTRODUCTION

1.1 Motivation

Over the past decade, electronic computing systems have permeated every aspect of people's lives. Smartphones and tablets are found in almost every household. Even the most basic smartphone contains computational power which exceeds the computing systems that put a man on the moon. Traditional banking and commerce also rely heavily on large, high-performance, secure, and robust centralized computing systems. Society is demanding that personal computing products be made smaller and more powerful, and that server and data center systems be made to handle high bandwidth and provide reliable computing performance. High-speed and compact computing systems have revolutionized the way education, health care, transportation, and national security services are delivered around the world.

From the engineer's perspective, computing systems are becoming increasingly large and complex in structure, and the demand for speed and bandwidth performance continues to rise. Higher-speed systems are especially sensitive to the effects of uncertainties, since small changes in physical or material parameters can have significant impact on the electrical performance of the system. Thus, it is increasingly important that the uncertainties in such systems be characterized using tools that can perform the task in a reasonable amount of time.

In the past several years, fast stochastic numerical techniques have been investigated heavily in the electronics packaging and electromagnetic compatibility communities for their abilities to solve problems involving uncertainties more efficiently than

Monte Carlo techniques [1, 2, 3, 4, 5, 6, 7, 8, 9]. The outputs from these uncertainty quantifications have been used to optimize designs [10, 11] and study problems with inherent uncertainties whose probability profiles have not been captured in the past [9].

The contribution of the work reported in this thesis is a more general and systematic way of simulating problems involving both electromagnetic extraction and circuit simulation. To this end, several stochastic computation approaches are investigated. A general-purpose stochastic circuit solver is presented to solve circuits with stochastic elements. And sampling-based approaches are used to perform uncertainty quantification using existing and mature electromagnetic solvers that are complicated to modify. Applying these techniques together enables simulation of multi-level systems involving uncertainties with reasonable computational resources.

1.2 Outline

This thesis begins with a review of current literature on fast stochastic numerical techniques in Chapter 2, both from a technique point of view in the applied mathematics field, and from an application point of view in the applied electromagnetics field. The formulation for several approaches to stochastic modeling and simulation is presented. The current challenges that these techniques currently face are also discussed.

The formulation for a transient circuit solver capable of solving stochastic circuit problems is presented in Chapter 3. The technique is based on finite-difference approximation of Kirchhoff's voltage and current laws in time domain. The application of two stochastic numerical techniques, both sampling and non-sampling, as they apply to this circuit solver, is discussed. An example illustrating the capabilities of the simulator is presented.

In Chapter 4, the stochastic circuit solver is used to solve transmission line problems involving uncertainty. The uncertainties in the problems manifest in the forms of randomness in the transmission line parameters, as well as randomness in the

physical construction of the lines. Methods for modeling these sources of uncertainties, as well as the simulation results are shown. A hybrid method of sampling and non-sampling method to perform modeling and simulation steps separately for more efficiency are presented.

Chapter 5 focuses on the application of sampling non-intrusive Stochastic Collocation method as it applies to multi-level electromagnetics and circuit simulations, and methods to increase the efficiency of random space sampling for cost functions that are resonant. A benefit of sampling techniques is that they allow problems involving complicated solvers to be used, and can be incorporated with well-developed commercial and proprietary solvers. However, often-times large problems lead to high-order solutions which may exhibit resonant or other non-smooth behavior in the random domain. The existence of such artifacts can make sampling techniques inaccurate and slow. Some techniques to address these challenges are discussed in this chapter. An example of a multi-level high-order simulation is presented to demonstrate the need for further technique improvements to address these types of problems. Another example is presented that uses adaptive wavelet interpolation to study a resonant RLC circuit.

Finally, a discussion of the work presented in this thesis, as well as future research directions based on the results, are provided in Chapter 6.

CHAPTER 2

BACKGROUND

2.1 Polynomial Chaos

Most of the modern fast stochastic numerical techniques are based on the concept of polynomial chaos expansion, first introduced by Norbert Wiener [12] in 1938 to expand Gaussian stochastic processes using Hermite polynomials Ψ_k.

$$X(\omega) = \sum_{k=0}^{\infty} x_k \Psi_k(\boldsymbol{\xi}(\omega)) \tag{2.1}$$

Orthogonal polynomials such as Hermite polynomials form a complete set of basis to approximate functionals in L_2 space. They satisfy the orthogonality condition:

$$\langle \Psi_i, \Psi_j \rangle = \left\langle \Psi_i^2 \right\rangle \delta_{ij} \tag{2.2}$$

where δ_{ij} is the Kronecker delta function:

$$\delta_{ij} = \begin{cases} 0 & \text{if } i \neq j \\ 1 & \text{if } i = j \end{cases} \tag{2.3}$$

The usefulness of using Hermite polynomials to represent Gaussian random variables comes from the definition of the inner product:

$$\langle f(\boldsymbol{\xi}), g(\boldsymbol{\xi}) \rangle = \int_{\Omega} f(\boldsymbol{\xi}) g(\boldsymbol{\xi}) W(\boldsymbol{\xi})\, d\boldsymbol{\xi} \tag{2.4}$$

where the weighting function $W(\boldsymbol{\xi})$ resembles the probability distribution function

Table 2.1: Hermite polynomials ψ_k for expansion of 4 random dimensions with order $p = 2$. [13]

k	p	ψ_k	$\langle \psi_k^2 \rangle$
0	0	1	1
1	1	ξ_1	1
2	1	ξ_2	1
3	1	ξ_3	1
4	1	ξ_4	1
5	2	$\xi_1^2 - 1$	2
6	2	$\xi_1\xi_2$	1
7	2	$\xi_1\xi_3$	1
8	2	$\xi_1\xi_4$	1
9	2	$\xi_2^2 - 1$	2
10	2	$\xi_2\xi_3$	1
11	2	$\xi_2\xi_4$	1
12	2	$\xi_3^2 - 1$	2
13	2	$\xi_3\xi_4$	1
14	2	$\xi_4^2 - 1$	2

of a normalized Gaussian random variable with mean 0 and unit variance:

$$W(\boldsymbol{\xi}) = \frac{1}{\sqrt{(2\pi)^n}} \exp(-\frac{1}{2}\boldsymbol{\xi}^T\boldsymbol{\xi}) \tag{2.5}$$

Table 2.1 shows Hermite polynomials for 4 random dimensions with expansion order $p = 2$, which is used in the examples in Chapters 3 and 4.

It is worth noting here that the random vector $\boldsymbol{\xi}$ can be multi-dimensional. The Gaussian distribution is assumed to be independent and identically distributed. The form of (2.4) allows the probabilistic moments of the random variables to be calcu-

lated directly from the expansion coefficients. Furthermore, it is shown in [14, 15, 16] that the expansion (2.1) converges almost exponentially fast, when the correct basis is chosen for the type of distribution and the function is sufficiently smooth in the random domain. In practice, this is significant since any practical computer code implementation of the expansion (2.1) will need to be truncated to a finite number of terms.

To this end, a more generalized formulation for Polynomial Chaos to deal with probability distributions other than Gaussian needs to be developed. Xiu and Karniadakis proposed in [14] to use the Askey-scheme to find different orthogonal polynomials for some common probability distributions. For instance, the Legendre polynomials can be used to expand uniformly distributed random variables, and Laguerre polynomials for gamma distributions such as exponential distribution and χ^2-distributions. The so-called generalized Polynomial Chaos (gPC) is central to several of the techniques discussed and implemented in this document.

In packaging electrical analysis applications, uniform random variables are useful for modeling quantities that are completely random by nature. Typically, there is not a target value for such parameters, and the value within a pre-defined range is equally acceptable. This can include parameters which the designer has no control over, but for which the range is well characterized. For instance, the relative position of PCB traces with respect to fiber-weave bundles on the substrate can be effectively modeled in as a uniformly distributed random variable.

Uniformly distributed random variables are best expanded using Legendre polynomials, listed in Table 2.2. The inner product of Legendre polynomials is defined as:

$$\langle f(\xi), \phi_k(\xi) \rangle = \int_{-1}^{1} f(x)\phi_k(\xi)\, d\xi = \int_{-\infty}^{\infty} f(x)\phi_k(\xi)W(\xi)\, d\xi \tag{2.6}$$

where the weighting function

$$W(\xi) = \begin{cases} \frac{1}{2} & \xi \in [-1, 1] \\ 0 & \text{otherwise} \end{cases} \tag{2.7}$$

Table 2.2: Legendre polynomials ϕ_k for expansion of 1 random dimension with order $p = 5$.

k	$\phi_k(\xi)$	$\langle \phi_k^2 \rangle$
0	1	2
1	ξ	$\frac{2}{3}$
2	$\frac{1}{2}(3\xi^2 - 1)$	$\frac{2}{5}$
3	$\frac{1}{2}(5\xi^3 - 3\xi)$	$\frac{2}{7}$
4	$\frac{1}{8}(35\xi^4 - 30\xi^2 + 3)$	$\frac{2}{9}$
5	$\frac{1}{8}(63\xi^5 - 70\xi^3 + 15\xi)$	$\frac{2}{11}$

is the PDF of a standard uniformly distributed random variable $\xi \sim \mathcal{U}(-1, 1)$. Any uniform random variable with distribution $C(\xi) \sim \mathcal{U}(a, b)$ can be normalized to a standard uniform random variable:

$$C(\xi) = \frac{1}{2}(a + b) + \frac{1}{2}(a - b)\xi \tag{2.8}$$

Legendre polynomials are orthogonal with respect to the inner product and weighting function defined in (2.6) and (2.7):

$$\langle \phi_k(\xi), \phi_l(\xi) \rangle = \int_{-\infty}^{\infty} \phi_k(\xi)\phi_l(\xi)W(\xi)\, d\xi = \frac{2}{2k + 1}\delta_{kl} \tag{2.9}$$

2.2 Non-Sampling Approaches

An approach to leveraging gPC expansion for solving problems with stochastic inputs is via Galerkin projection. The Stochastic Galerkin Method (SGM) is considered an intrusive, or non-sampling technique. This means that the gPC expansion needs to be taken into consideration when developing code for solving the underlying physical problem, and hence existing codes cannot be used directly with this technique. The technique was proposed by Ghanem and Spanos [13].

To begin, every random variable is approximated using a truncated gPC expansion:

$$u(x,t,\omega) = \sum_{k=0}^{P} u_k(x,t)\Psi_k(\boldsymbol{\xi}(\omega)) \tag{2.10}$$

For a differential system $\mathcal{L}(\cdot)$

$$\frac{\partial}{\partial t}u(x,t,\omega) = \mathcal{L}(u) \tag{2.11}$$

with corresponding boundary conditions and initial conditions, the problem is solved numerically by taking the inner product of both sides of the equation with testing functions, in this case using the same polynomials as the gPC basis functions:

$$\left\langle \frac{\partial}{\partial t}\sum_{k=0}^{P} u_k(x,t)\Psi_k(\omega), \Psi_k(\omega) \right\rangle = \left\langle \mathcal{L}(\sum_{k=0}^{P} u_k(x,t)\Psi_k(\omega)), \Psi_k(\omega) \right\rangle \tag{2.12}$$

applied for all $|k| \leq P$. Using the corresponding gPC basis functions Ψ_k, the inner products are essentially calculating expectations in the random domain, thus removing any ω dependency in the problem. The problem becomes a matrix system that can be numerically solved using a computer.

The solution obtained is the gPC expansion coefficients $u_k(x,t)$, which can then be used to calculate the statistics of the response, or re-form the stochastic solution by substituting in (2.10).

The size of the system for a given random dimension d is $\begin{pmatrix} P+d \\ P \end{pmatrix}$, and the parameters are coupled so the system matrix is dense. We see that the size of the problem grows unfavorable with respect to both the dimensionality of random space, and the chosen order of gPC truncation. However, the stochastic solution is obtained by solving only one matrix equation, and with the correct gPC basis function, the solution is optimally accurate for the computational complexity.

SGM has been utilized in the electrical packaging community to model chip and board-level multi-conductor transmission lines [8], through-silicon vias (TSVs)[2],

and solve circuits [17, 18], and has also been used in the electromagnetics community [19] to solve some specific problems. However, due to the intrusive nature of the technique, new solver code needs to be developed and hence most of the aforementioned studies have implemented application-specific code for solving the respective problems.

2.3 Sampling Approaches

Unlike intrusive approaches such as SGM, sampling approaches work with existing solvers for the problems being studied. Hence this class of techniques is called non-intrusive, and the stochastic computation is uncoupled from the system solver.

The classic sampling approach is Monte Carlo (MC), where a set of random inputs is generated based on some random distribution, then the solution is repeatedly obtained using deterministic solvers. All the outputs are collected and used to calculate statistics.

1. Choose a sample size N. Generate N i.i.d. random variables $\{X_i(\omega_j)\}_{j=1}^{d}$ for $i = 1, ..., N$. Here d is the dimension of the random input vector.

2. For each i, solve deterministic problem to obtain output $\{Y_i(\omega_j)\}_{j=1}^{d'}$ where d' is the dimension of the output vector.

3. Calculate statistics from the set of all $\{Y_i(\omega_j)\}_{j=1}^{d'}$ for $i = 1, ..., N$.

The convergence rate for Monte Carlo is asymptotically $\frac{1}{\sqrt{N}}$, which means the number of runs necessary can increase dramatically if higher accuracy is desired. However, Monte Carlo sampling converges independent of the input dimensionality d. This could make Monte Carlo a viable method for cases where the number of independent random inputs is large.

In comparison, Stochastic Collocation (SC) is a sampling method that is more structured and hence may be more efficient for problems of manageable dimensionality. To perform SC, rather than sampling the random space over a set of random

samples, the deterministic simulation is instead performed over a set of collocation nodes $\Theta_d = \{x_i\}_{i=1}^M$ defined over a finite region of the random space. An interpolation is then constructed over the space defined by this set of nodes to construct an interpolation of the response of interest:

$$\mathcal{I}(u)(x) = \sum_{i=1}^{M} f(x_i) L_i(x_i) \tag{2.13}$$

where the L_i are Lagrange polynomials for interpolation. The statistics of the response are then constructed via integration over the interpolation, either through Monte Carlo sampling of the interpolation $\mathcal{I}(u)(x)$ or quadrature rule defined over the random space.

Any potential speed-up from SC vs. MC comes from the choice of collocation points and construction of the interpolation. The most straightforward is to use tensor product of node sets generated by one-dimensional rule. Linearly transform a random dimension into standardized support $[-1, 1]$, then a one-dimensional node set is:

$$\Theta_1^i = (x_1^i, ..., x_{m_i}^i) \subset [-1, 1] \tag{2.14}$$

Such a node set can be defined uniformly spaced, or using some polynomial interpolation scheme such as Clenshaw-Curtis. Then, for the entire $d-$dimensional space, the interpolation can be constructed:

$$\mathcal{I}(u)(x) = \sum_{k_1=1}^{m_{i1}} \cdots \sum_{k_d=1}^{m_{id}} f(x_{k_1}^{i_1}, ..., x_{k_d}^{i_d}) \cdot (a_{k_1}^{i_1} \otimes \cdots \otimes a_{k_d}^{i_d}) \tag{2.15}$$

which requires that a system of $m_{i1} \times \cdots \times m_{i_d}$ of collocation nodes needs to be evaluated. Assuming that there are N number of nodes in each dimension, then the total number of deterministic simulations needed is $M = N^d$. This is unfavorable for problems with even moderate dimensionality, especially if the function is so complicated that more points are needed in each dimension to resolve the features.

A more efficient interpolation scheme for moderate-dimensional problems is the

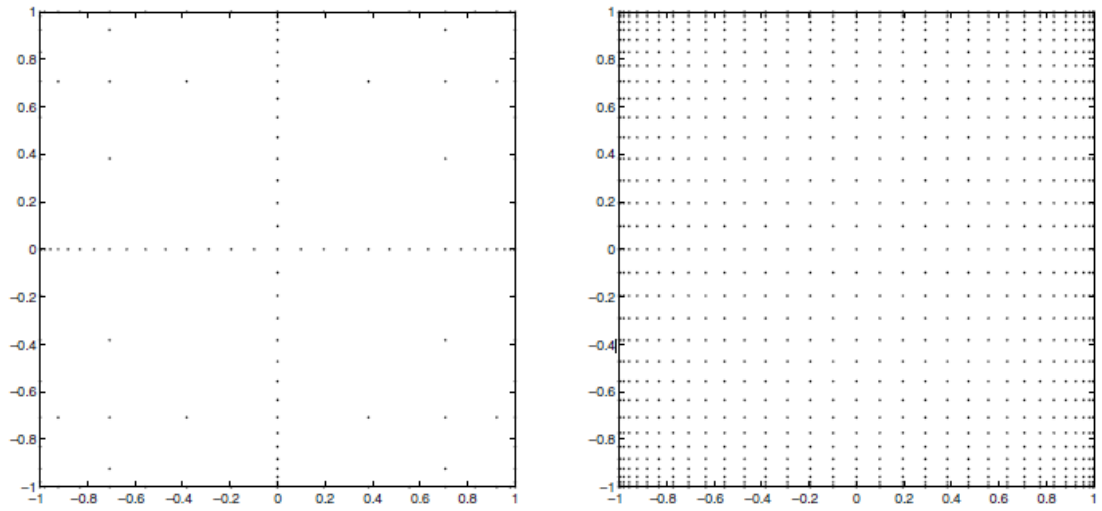

Figure 2.1: Sparse grid vs. full tensor-product grid for $d = 2$ case and $k = 5$. The one-dimensional rules of both grids are equivalent, but the sparse grid has 145 nodes whereas the full tensor product grid requires 1089 nodes. [20]

Smolyak sparse grid. Instead of requiring all the nodes in the tensor product grid, a more efficient method is used to choose the nodes. The interpolation of some level k requires a set of sparse nodes:

$$\Theta_d = \bigcup_{q-d+1 \leq |\boldsymbol{i}| \leq q} \left(\Theta_1^{i_1} \times \cdots \times \Theta_1^{i_d}\right) \tag{2.16}$$

where $q = d + k$ and the total number of deterministic nodes that needs to be evaluated is proportional to $\frac{2^k}{k!}d^k$ for fixed k and $d \gg 1$. k is known as the "level" of interpolation. A comparison of tensor product grid vs. sparse grid using the same one-dimensional rule is shown in Figure 2.1. These figures are generated using Clenshaw-Curtis rule in 1D, which corresponds to roots of the Chebyshev polynomial. In practice, a uniform rule or Gaussian rule can also be used.

2.4 Dimensionality Reduction

Both the intrusive and non-intrusive approaches presented in the sections above suffer from the "curse of dimensionality". The size of the problem grows superlinearly with respect to the dimensionality of random space for both approaches. Interestingly, Monte Carlo sampling does not suffer from this problem, and is actually the preferred method for problems with very high dimensionality ($d > 15$).

Hence, the value of these fast stochastic computation techniques can only be realized if the dimensionality of the random space is manageable. Fortunately, this is often the case. Even when the number of random parameters in a problem is high, the underlying source of uncertainty is often attributed to a small set of random parameters. For instance, uncertainties in the dielectric properties of substrates can lead to uncertainties in several transmission line parameters, but the underlying random space has only dimensionality one. Any process variations in manufacturing a package or board are likely to result from either over or under-exposure of the raw substrate to the etching process. Therefore in the case of multiple transmission lines, although there are uncertainties associated with the width and height of each line, these parameters are expected to be strongly correlated since all the lines are etched on the same substrate during the same process. In this case, the underlying random space is still low.

Mathematically, the fact that many random parameters result from variations in a single process implies that the correlation of all random parameters should be leveraged to minimize the dimensionality of the underlying random space. This has been achieved through the use of Principal Component Analysis (PCA) [4, 5], which projects the random spaces into orthogonal subspaces, and removes the dimensions that have the least effect on the overall system. Other approaches [21, 22, 23] such as HDMR have also been considered. The dimensionality can be reduced through these mathematical techniques, or through knowledge of the underlying physical phenomena that lead to the uncertainties.

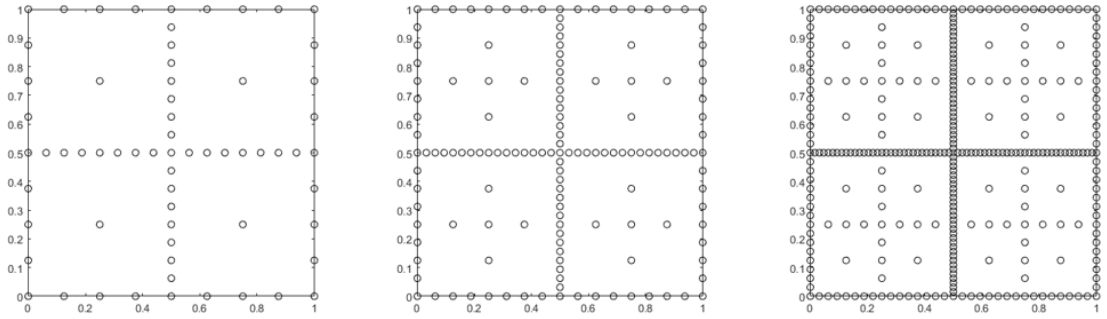

Figure 2.2: Nesting structure of $d = 2$ Smolyak sparse grids. Levels $k = \{4, 5, 6\}$ are shown.

2.5 Adaptive Mesh Refinement

Stochastic Collocation can also be accelerated through adaptive mesh refinement of the sparse grid [24, 25]. An advantage of the Smolyak sparse grid is that the nodes exhibit level-wise nested behavior, as shown in Figure 2.2. Hence each subsequent level of interpolation uses nodes from the previous level. This allows for multiple mechanics of mesh refinement, so that for a given accuracy level, the smallest level of interpolation and hence the least number of deterministic simulations are needed. If a method to evaluate the quality of interpolation can be implemented, then the mesh can be refined adaptively in this fashion.

Refinement can be achieved in three ways:

1. **Level refinement** - increasing the level k of interpolation [26]. The hierarchical structure of sparse grid construction allows additional interpolation nodes to be added to the grid, which are used along with existing nodes to create more accurate interpolation of the cost function. This type of refinement is demonstrated in Figure 2.2.

2. **Anisotropic refinement** - increasing the number of nodes along dimensions with the highest sensitivity to the output of interest. This would achieve a result similar to that of dimensionality reduction [27] in the sense that more computational resource is dedicated to inputs with the highest impact on the

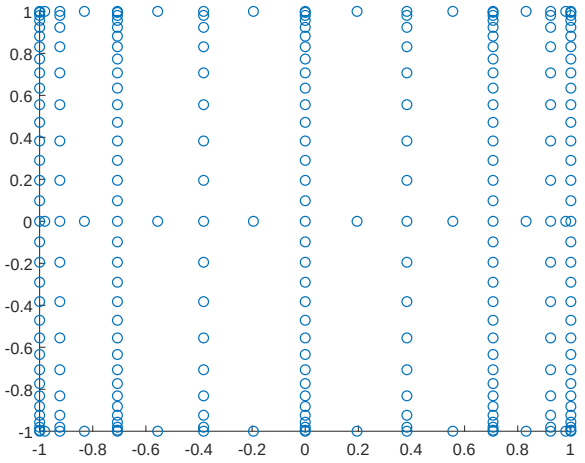

Figure 2.3: Example of an anisotropically refined sparse grid.

output. An example of a sparse grid anisotropically refined is shown in Figure 2.3.

3. **Local mesh refinement** - adding nodes where the function is non-smooth to increase the precision of interpolation in that region, without needing to add additional points over the entire random domain [28]. This method requires an iterative scheme to determine which nodes need further refinement. The interpolation for local refinement can be performed using local polynomials or wavelets. An example of a locally refined sparse grid is shown in Figure 2.4.

In Chapter 5 of this thesis, a local refinement scheme using wavelet basis for interpolation is considered to perform SC on a problem with resonance in the output function.

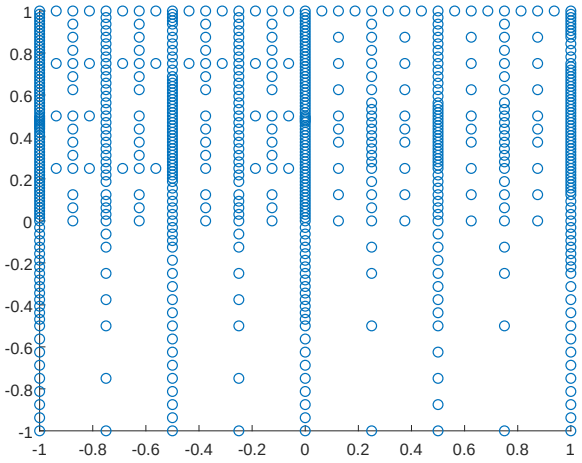

Figure 2.4: Example of a locally refined sparse grid.

CHAPTER 3

STOCHASTIC LIM

3.1 Introduction

In recent years, fast stochastic computational methods have been steadily gaining interest in the packaging community for enabling electrical modeling and simulation with uncertainties [8, 29, 5, 30, 10]. Modern stochastic numerical techniques include non-intrusive methods such as Monte Carlo (MC) sampling [31] and Stochastic Collocation (SC) [20, 15, 16], which work with existing PDE solvers; intrusive methods such as Stochastic Galerkin Method (SGM) [16, 13] require the underlying PDE solver to be re-formulated to include expansion of random variables. Though more cumbersome to implement, SGM is optimally accurate with finite terms of expansion since the residue is always orthogonal to the space spanned by the polynomial basis [16].

SGM has been utilized for performing stochastic circuit simulations [17, 32], including transmission lines [8] and nonlinear devices [30, 17]. This chapter presents a transient solver for stochastic circuits based on the Latency Insertion Method (LIM) [33, 34] using time-domain finite-difference scheme. The finite-difference time domain (FDTD) method for computational electromagnetics, on which LIM is based, has been shown to be effective for propagating uncertainty [35, 36]. Due to its simple formulation and linear computational complexity with respect to size of state space, LIM is an ideal application for SGM.

The function of Stochastic LIM is to provide a transient simulator for circuits with random variables as parameters. The simulator takes a circuit netlist as its input,

where some of the parameter values in the deck are random variables, and performs fast probabilistic calculations using stochastic numerical techniques. The output of the simulator is the probability distribution function (PDF) of voltage or current at a specified node or branch on the circuit. Compared with typical deterministic circuit solvers, where the time-domain solution is the exact solution to the set of differential equations governing the given circuit, stochastic circuit solvers such as Stochastic LIM calculate the statistics of the response as it evolves over time.

Traditionally, statistical simulation of circuits is performed using Monte Carlo sampling of outputs from deterministic circuit solvers. In such procedures, the probability distributions of random parameters of interest are first defined. A random generator is then used to generate N samples based on the prescribed distribution. Let $X = \{X_i\}_{i=1}^N$ denote the set of random samples, where X_i are independent identically distributed random vectors generated by the random generator. Then, a circuit netlist is constructed for each X_i and simulated, with the output denoted by $Y = \{Y_i\}_{i=1}^N$ where each Y_i corresponds to the output from input X_i from either LIM or another solver.

The statistics of the response are then computed from the complete set of outputs. For instance, the sampled mean can be calculated as

$$\mathbb{E}[Y] \approx \frac{1}{N} \sum_{i=1}^{N} Y_i \tag{3.1}$$

and the sampled variance can be calculated as

$$\mathrm{Var}[Y] = \sigma^2 \approx \frac{1}{N-1} \sum_{i=1}^{N} (Y_i - \mathbb{E}[Y])^2 \tag{3.2}$$

For both cases, the calculated value is merely an estimate of the actual statistical moments for any finite N. In fact, the sampled mean is itself a Gaussian random variable with distribution $\mathcal{N}(\mathbb{E}[X], \frac{\sigma^2}{N})$. Therefore, the standard error of the sampled mean is $\sigma_{\bar{x}} = \frac{\sigma}{\sqrt{N}}$. This implies that the accuracy of the estimated mean converges at a rate of $\frac{1}{\sqrt{N}}$ for Monte Carlo sampling. To gain accuracy, an increasingly large

sample size must be simulated, which is undesirable or intractable in most circumstances.

This chapter first presents the formulation for Stochastic LIM using Polynomial Chaos (PC) expansion and SGM. The formulation is then verified by comparing simulation results of a random resistor network against MC sampling using deterministic LIM. Due to the time-domain nature of LIM, the method works well with arbitrary excitations, including sources that are non-smooth in time.

3.2 Deterministic LIM

LIM is a finite-difference time-domain circuit solver that is similar to the FDTD method for electromagnetics [33]. The circuit to be simulated is defined in terms of nodes and branches. The topologies for nodes and branches are shown in Figure 3.1. At each node, there must be a finite capacitance to ground, and each branch must contain a finite inductance in series to ensure that there is latency in the circuit and the time-domain simulation can be performed subject to a conditionally stable criterion [37]. This requirement is naturally satisfied for transmission line-type simulation, where the latencies resulting from capacitance and inductance are inherent to the structure.

At each node, the semi-implicit Kirchhoff's current law is:

$$C_i \left(\frac{V_i^{n+\frac{1}{2}} - V_i^{n-\frac{1}{2}}}{\Delta t} \right) + \frac{G_i}{2} \left(V_i^{n+\frac{1}{2}} + V_i^{n-\frac{1}{2}} \right) - H_i^n = -\sum_{j=1}^{M_i} I_{ij}^n \tag{3.3}$$

where the superscript $n \pm \frac{1}{2}$ is the time index for voltages, and the subscript i is the nodal index. The subscripts ij represent branch current that connects the nodes i and j. There are a total of M_i branches connected to node i. Similar to the electric and magnetic fields in FDTD, the time indexes of voltages and currents are offset by a half time step, hence the $\pm\frac{1}{2}$ term in time index for voltage values.

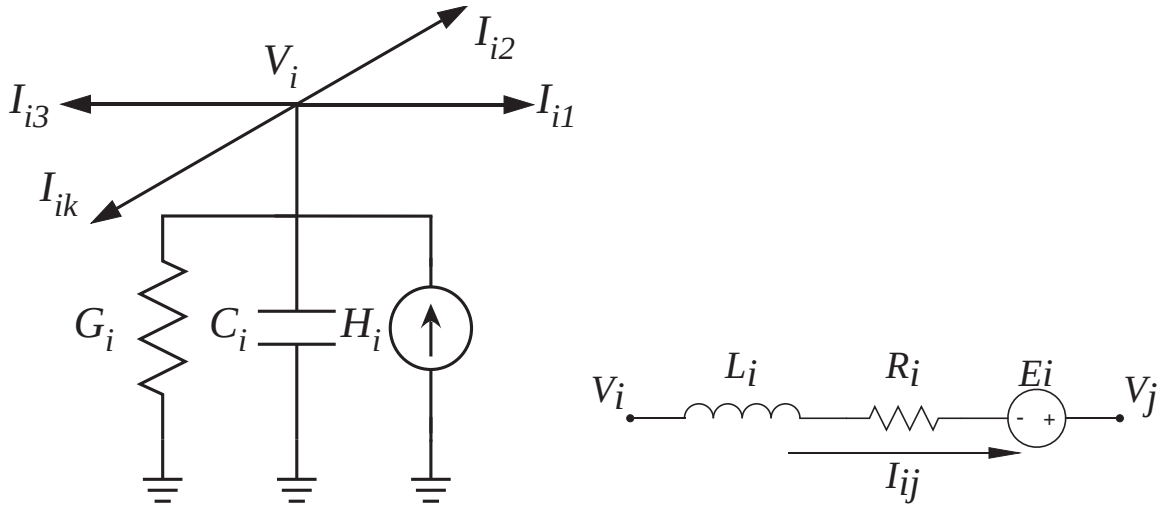

(a) Node topology (b) Branch topology

Figure 3.1: Node and branch topology for Latency Insertion Method.

The semi-implicit LIM form of Kirchhoff's voltage law at each branch is:

$$V_i^{n+\frac{1}{2}} - V_j^{n+\frac{1}{2}} = L_{ij}\left(\frac{I_{ij}^{n+1} - I_{ij}^{n}}{\Delta t}\right) + \frac{R_{ij}}{2}\left(I_{ij}^{n+1} + I_{ij}^{n}\right) - E_{ij}^{n+\frac{1}{2}} \tag{3.4}$$

3.3 Stochastic Galerkin Method Approach

3.3.1 Polynomial Chaos Expansion

We first expand the circuit elements and voltage/current values using Generalized Polynomial Chaos (gPC) basis:

$$V_i(\omega) = \sum_{k=0}^{P} V_{i,k}\,\psi_k(\boldsymbol{\xi}(\omega)) \tag{3.5}$$

$$I_{ij}(\omega) = \sum_{k=0}^{P} I_{ij,k}\, \psi_k(\boldsymbol{\xi}(\omega)) \tag{3.6}$$

$$G_i(\omega) = \sum_{k=0}^{P} G_{i,k}\, \psi_k(\boldsymbol{\xi}(\omega)) \tag{3.7}$$

$$C_i(\omega) = \sum_{k=0}^{P} C_{i,k}\, \psi_k(\boldsymbol{\xi}(\omega)) \tag{3.8}$$

$$R_{ij}(\omega) = \sum_{k=0}^{P} R_{ij,k}\, \psi_k(\boldsymbol{\xi}(\omega)) \tag{3.9}$$

$$L_{ij}(\omega) = \sum_{k=0}^{P} L_{ij,k}\, \psi_k(\boldsymbol{\xi}(\omega)) \tag{3.10}$$

where $V_i(\omega)$, $G_i(\omega)$, $C_i(\omega)$ are the random nodal voltage, conductance, and capacitance values at node i, and $I_{ij}(\omega)$, $R_{ij}(\omega)$, and $L_{ij}(\omega)$ are the random branch current, resistance, and inductance values at branch ij, respectively. $\omega \in \Omega$ is an event in probability space of dimension d, $\boldsymbol{\xi}(\omega) = [\xi_1(\omega), \xi_2(\omega), \cdots, \xi_d(\omega)]^T$ is the vector of i.i.d random variables, and $\psi_k(\cdot)$ are the generalized Polynomial Chaos (gPC) basis functions, satisfying the orthogonality condition:

$$\langle \psi_k, \psi_l \rangle = \langle \psi_k^2 \rangle\, \delta_{kl} \tag{3.11}$$

It is helpful to standardized the random variables ξ_i when performing gPC expansion. This is due to the fact that the weighting functions associated with Hermite and Legendre polynomials are the probability density functions of standardized Gaussian and uniform random variables, respectively. The dimensionality d of the random space is the number of independent random parameters that affect the outcome.

Some choices of PC basis used in the expansion are Hermite polynomials and Legendre polynomials, the properties of which are discussed in Section 2.1.

3.3.2 Node Algorithm

We start with (3.3). By moving the $n-\frac{1}{2}$ terms to the right-hand side, and inserting the expansions in (3.5), (3.6), (3.7) and (3.8), we obtain:

$$\sum_{k=0}^{P}\sum_{l=0}^{P}\left[\left(\frac{C_{i,k}}{\Delta t}+\frac{G_{i,k}}{2}\right)V_{i,l}^{n+\frac{1}{2}}\right]\psi_k(\boldsymbol{\xi})\psi_l(\boldsymbol{\xi}) = \sum_{k=0}^{P}\sum_{l=0}^{P}\left[\left(\frac{C_{i,k}}{\Delta t}-\frac{G_{i,k}}{2}\right)V_{i,l}^{n-\frac{1}{2}}\right]\psi_k(\boldsymbol{\xi})\psi_l(\boldsymbol{\xi}) + \sum_{k=0}^{P}\left(H_{i,k}^{n}-\sum_{j=1}^{M_i}I_{ij,k}^{n}\right)\psi_k(\boldsymbol{\xi}) \quad (3.12)$$

The system of equations describes the relationships between gPC expansion coefficients of circuit elements, voltage and current values. To solve these equations numerically, we perform Galerkin projection by taking the inner product on both sides with the respective gPC polynomials used in the expansion, which results in:

$$\sum_{k=0}^{P}\sum_{l=0}^{P}\left[\left(\frac{C_{i,k}}{\Delta t}+\frac{G_{i,k}}{2}\right)V_{i,l}^{n+\frac{1}{2}}\right]\langle\psi_k(\boldsymbol{\xi}),\psi_l(\boldsymbol{\xi}),\psi_m(\boldsymbol{\xi})\rangle = \sum_{k=0}^{P}\sum_{l=0}^{P}\left[\left(\frac{C_{i,k}}{\Delta t}-\frac{G_{i,k}}{2}\right)V_{i,l}^{n-\frac{1}{2}}\right]\langle\psi_k(\boldsymbol{\xi}),\psi_l(\boldsymbol{\xi}),\psi_m(\boldsymbol{\xi})\rangle + \left(H_{i,m}^{n}-\sum_{j=1}^{M_i}I_{ij,m}^{n}\right)\left\langle\psi_m^2(\boldsymbol{\xi})\right\rangle, \quad m=0,1,...,P \quad (3.13)$$

The triple inner product in the above equation is the integral:

$$\langle\psi_k(\boldsymbol{\xi}),\psi_l(\boldsymbol{\xi}),\psi_m(\boldsymbol{\xi})\rangle = \int_{\mathbb{R}^d}\psi_k(\boldsymbol{\xi})\psi_l(\boldsymbol{\xi})\psi_m(\boldsymbol{\xi})W(\boldsymbol{\xi})\,d\boldsymbol{\xi} \quad (3.14)$$

which can be evaluated analytically or using a multi-dimensional quadrature rule. It should be noted that these triple inner products are problem-independent, and only

need to be solved once for all problems with a given number of random dimensions and expansion order. Hence, these values do not need to be calculated during each simulation.

Putting (3.13) into matrix form, we find the explicit nodal voltage update equation for $\mathbf{V}_i^{n+\frac{1}{2}}$ to the left-hand side:

$$\mathbf{V}_i^{n+\frac{1}{2}} = \left(\frac{\mathbf{C}_i}{\Delta t} + \frac{\mathbf{G}_i}{2}\right)^{-1} \times \left[\left(\frac{\mathbf{C}_i}{\Delta t} - \frac{\mathbf{G}_i}{2}\right)\mathbf{V}_i^{n-\frac{1}{2}} + \mathbf{H}_i^n - \sum_{j=1}^{M_i} \mathbf{I}_{ij}^n\right] \tag{3.15}$$

$$\mathbf{V}_i^{n+\frac{1}{2}} = \left[V_{i,0}^{n+\frac{1}{2}}, V_{i,1}^{n+\frac{1}{2}}, \cdots, V_{i,P}^{n+\frac{1}{2}}\right]^T \tag{3.16}$$

$$\mathbf{I}_{ij}^n = \left[I_{ij,0}^n, I_{ij,1}^n, \cdots, I_{ij,P}^n\right]^T \tag{3.17}$$

$$\mathbf{S}_k = \begin{bmatrix} \frac{\langle\psi_k,\psi_0,\psi_0\rangle}{\langle\psi_0^2\rangle} & \frac{\langle\psi_k,\psi_0,\psi_1\rangle}{\langle\psi_0^2\rangle} & \cdots & \frac{\langle\psi_k,\psi_0,\psi_P\rangle}{\langle\psi_0^2\rangle} \\ \frac{\langle\psi_k,\psi_1,\psi_0\rangle}{\langle\psi_1^2\rangle} & \ddots & & \vdots \\ \vdots & & \ddots & \vdots \\ \frac{\langle\psi_k,\psi_P,\psi_0\rangle}{\langle\psi_P^2\rangle} & \frac{\langle\psi_k,\psi_P,\psi_1\rangle}{\langle\psi_P^2\rangle} & \cdots & \frac{\langle\psi_k,\psi_P,\psi_P\rangle}{\langle\psi_P^2\rangle} \end{bmatrix} \tag{3.18}$$

$$\mathbf{C}_i = \sum_{k=0}^{P} C_{i,k}\mathbf{S}_k, \quad \mathbf{G}_i = \sum_{k=0}^{P} G_{i,k}\mathbf{S}_k \tag{3.19}$$

Here the expansion matrix $\mathbf{S}_k$ encapsulates all the triple inner products calculated a-priori, and can be easily used to calculate $\mathbf{C}_i$ and $\mathbf{G}_i$ matrices for all problems from the gPC expansion coefficients of $C_i(\boldsymbol{\xi})$ and $G_i(\boldsymbol{\xi})$. We will discuss how these expansion coefficients can be obtained in Section 4.1.

3.3.3 Branch Algorithm

We start with (3.4). By moving the n terms to the right-hand side and substituting in gPC expansion from (3.5), (3.6), (3.9) and (3.10), we obtain:

$$\sum_{k=0}^{P}\sum_{l=0}^{P}\left[\left(\frac{L_{ij,k}}{\Delta t}+\frac{R_{ij,k}}{2}\right)I_{ij,l}^{n+1}\right]\psi_k(\boldsymbol{\xi})\psi_l(\boldsymbol{\xi})$$
$$=\sum_{k=0}^{P}\sum_{l=0}^{P}\left[\left(\frac{L_{ij,k}}{\Delta t}-\frac{R_{ij,k}}{2}\right)I_{ij,l}^{n}\right]\psi_k(\boldsymbol{\xi})\psi_l(\boldsymbol{\xi})$$
$$+\sum_{k=0}^{P}\left(E_{ij,k}^{n+\frac{1}{2}}+V_{i,k}^{n+\frac{1}{2}}-V_{j,k}^{n+\frac{1}{2}}\right)\psi_k(\boldsymbol{\xi}) \quad (3.20)$$

Performing the Galerkin procedure by taking the inner product of both sides with the same gPC basis polynomial, we get a set of algebraic equations:

$$\sum_{k=0}^{P}\sum_{l=0}^{P}\left[\left(\frac{L_{ij,k}}{\Delta t}+\frac{R_{ij,k}}{2}\right)I_{ij,l}^{n+1}\right]\langle\psi_k(\boldsymbol{\xi}),\psi_l(\boldsymbol{\xi}),\psi_m(\boldsymbol{\xi})\rangle$$
$$=\sum_{k=0}^{P}\sum_{l=0}^{P}\left[\left(\frac{L_{ij,k}}{\Delta t}-\frac{R_{ij,k}}{2}\right)I_{ij,l}^{n}\right]\langle\psi_k(\boldsymbol{\xi}),\psi_l(\boldsymbol{\xi}),\psi_m(\boldsymbol{\xi})\rangle$$
$$+\left(E_{ij,k}^{n+\frac{1}{2}}+V_{i,k}^{n+\frac{1}{2}}-V_{j,k}^{n+\frac{1}{2}}\right)\left\langle\psi_m^2(\boldsymbol{\xi})\right\rangle, \quad m=0,1,...,P \quad (3.21)$$

Once again, the pre-calculated Galerkin expansion matrices $\mathbf{S}_k$ from (3.18) can be used to obtain the expanded matrices for L and R, resulting in an explicit update equation for $\mathbf{I}_{ij}^{n+1}$ in matrix form:

$$\mathbf{I}_{ij}^{n+1}=\left(\frac{\mathbf{L}_{ij}}{\Delta t}+\frac{\mathbf{R}_{ij}}{2}\right)^{-1}\times\left[\left(\frac{\mathbf{L}_{ij}}{\Delta t}-\frac{\mathbf{R}_{ij}}{2}\right)\mathbf{I}_{ij}^{n}+\mathbf{E}_{ij}^{n+\frac{1}{2}}+\mathbf{V}_{i}^{n+\frac{1}{2}}-\mathbf{V}_{j}^{n+\frac{1}{2}}\right] \quad (3.22)$$

$$\mathbf{R}_{ij}=\sum_{k=0}^{P}R_{ij,k}\mathbf{S}_k, \quad \mathbf{L}_{ij}=\sum_{k=0}^{P}L_{ij,k}\mathbf{S}_k \quad (3.23)$$

3.3.4 Simulation Procedure

To simulate a circuit with uncertainties using Stochastic LIM, use the following procedure:

1. Obtain gPC expansion coefficients for G, C, H at each node, and R, L, E at each branch. If the variable is deterministic, then the 1st expansion is the deterministic value, and all other expansion coefficients are 0. A procedure to obtain the expansion coefficients is presented in Section 4.1.

2. For each R, L, G, C, calculate Galerkin expanded matrices using (3.19) and (3.23).

3. For each time step n:

   (a) For each node, update voltage at time step $n + \frac{1}{2}$ using (3.15).

   (b) For each branch, update branch current at time step $n + 1$ using (3.22).

4. Post-process results to obtain response statistics.

The results from Stochastic LIM simulation are the gPC expansion coefficients of nodal voltages and branch currents at all time steps. The statistics of these responses can be obtained from post-processing of the coefficients:

$$\mathbb{E}[V_i^n] = V_{i,0}^n, \quad \sigma(V_i^n) = \sqrt{\sum_{k=1}^{P} V_{i,k}^n \langle \psi_k^2 \rangle} \tag{3.24}$$

The total amount of data that needs to be stored and post-processed is P times the number of time steps, where P is the terms in the gPC expansion. As we can see from examples in Section 3.3.5, this number is small for problems with manageable random dimensions. This means that Stochastic LIM generates a more compact data set and minimizes post-processing necessary to gather statistics when compared with Monte Carlo, where N times the number of time steps of data need to be stored, and typically $N \gg P$.

3.3.5 Numerical Example: Resistor Network

We test the Stochastic LIM formulation by simulating a purely resistive network. The circuit is shown in Figure 3.2a, and we choose the four resistors to ground to be independent Gaussian random variables. In order to perform simulation with LIM, small fictitious capacitance and inductance values need to be inserted at every node and branch, respectively. The augmented network is shown in Figure 3.2b. The values for all the circuit elements are listed in Figure 3.2. To increase accuracy, the capacitance and inductance values can be scaled by a factor of s, but the time step size Δt will also need to be scaled in order to satisfy the CFL stability condition, resulting in longer simulation time. The network is excited by a trapezoidal current source at node 1 with time delay $t_d = 1$ns, rise/fall time $t_{rf} = 1$ns, pulse width $t_w = 20$ns, and amplitude $I_{max} = 1$A. For $s = 1$, the mean and standard deviation of transient voltages at nodes 1 and 4 are shown in Figure 3.3. It can be seen that results from Stochastic LIM are almost identical to results using Monte Carlo with sample size $N = 10000$, while requiring only one simulation of the augmented system with $(P + 1)$ times more state variables. By choosing a small scaling factor $s = 0.1$, the circuit becomes almost purely resistive. As shown in Figure 3.4, good correlation is still observed between Stochastic LIM and MC when the waveform is non-smooth.

3.4 Stochastic Collocation Approach

Stochastic Collocation is a non-intrusive sampling technique, and thus the implementation of Stochastic LIM with SC more closely resembles Monte Carlo than SGM. In this case, the regular deterministic formulation of LIM will suffice. An external sparse grid interpolation routine [26, 38, 39, 40] is used to generate a set of collocation nodes. An efficient node set in $N-$dimensional space can be generated using the Smolyak algorithm.

Let us denote the set of sparse nodes by Θ_M. For each node $Z_i \in \Theta_M$, the vector Z_i contains an instantiation in the random space, and thus represents the input of a deterministic simulation. Let $Y_{i,t} = f_t(Z_i)$ where $f_t(\cdot)$ is the result from LIM at time

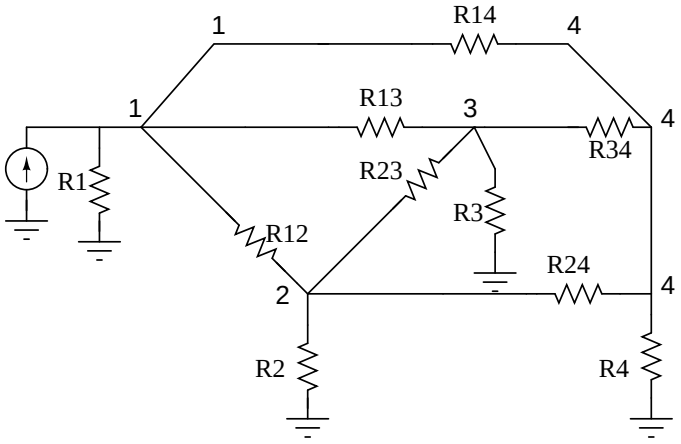

(a) Purely resistive circuit with no latency.

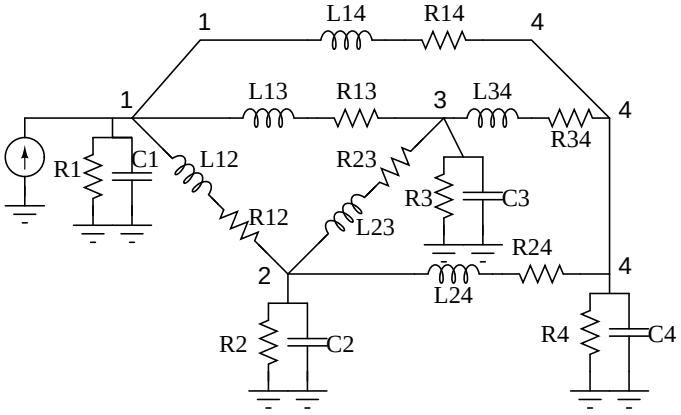

(b) Resistive circuit with inserted latencies for simulation with LIM.

Figure 3.2: Circuit diagram of resistor network used in example. The element values are: $R_{12} = 14.53\Omega, R_{13} = 4.53\Omega, R_{14} = 5.3\Omega, R_{23} = 25.3\Omega, R_{24} = 47.3\Omega, L_{12} = 32.4\text{nH}, L_{13} = 22\text{nH}, L_{14} = 32.2\text{nH}, L_{23} = 32.2\text{nH}, L_{24} = 43.2\text{nH}, C_1 = 10\text{pF}, C_2 = 20\text{pF}, C_3 = 20\text{pF}, C_4 = 0.2\text{pF}$. The resistors to ground are Gaussian random variables: $R_1(\omega) = (50 + 5\xi_1)\Omega, R_2(\omega) = (10 + 1\xi_2)\text{M}\Omega, R_3(\omega) = (10 + 1\xi_3)\text{M}\Omega, R_4(\omega) = (50 + 5\xi_4)\Omega$.

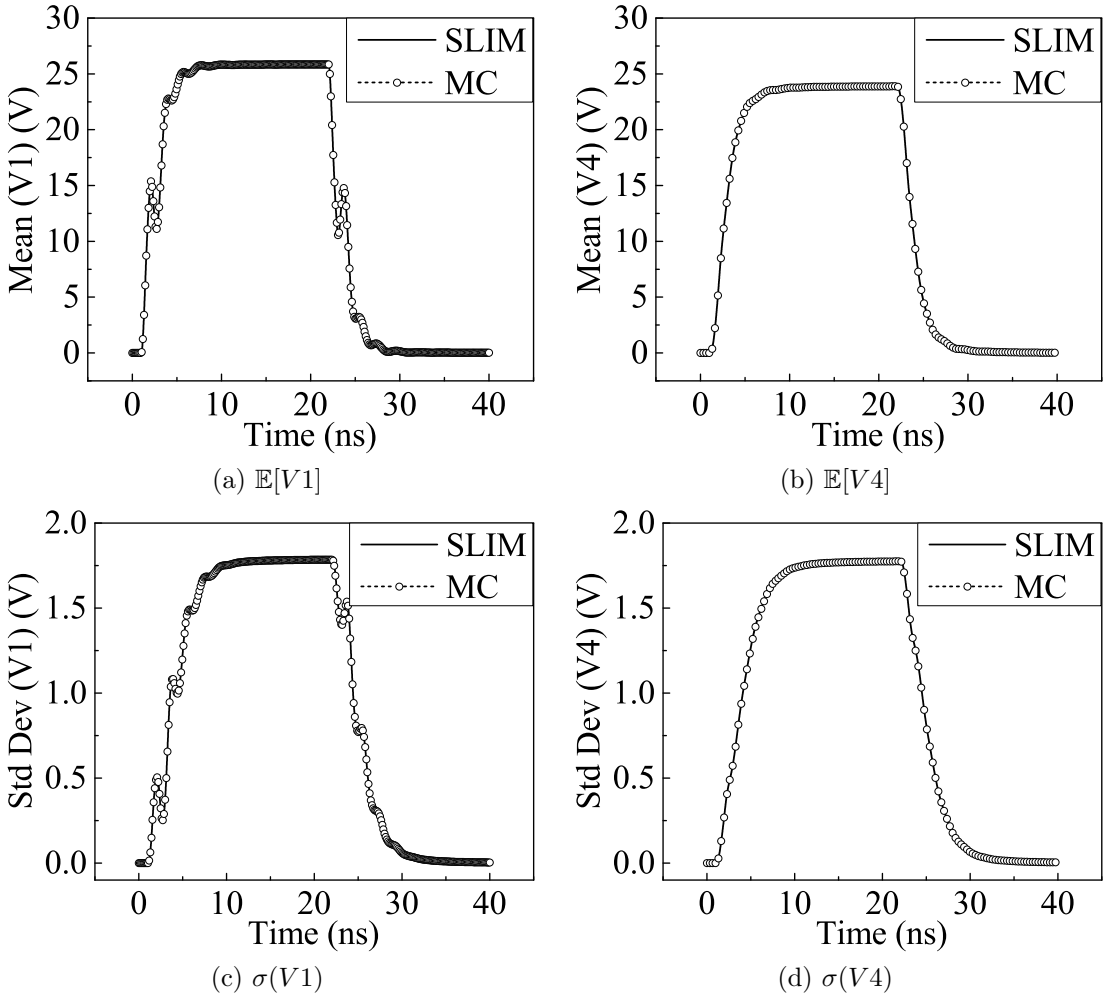

(a) $\mathbb{E}[V1]$ (b) $\mathbb{E}[V4]$

(c) $\sigma(V1)$ (d) $\sigma(V4)$

Figure 3.3: Stochastic LIM vs. Monte Carlo results for example shown in Figure 3.2 with scaling factor $s = 1$. The mean and standard deviation show excellent agreement.

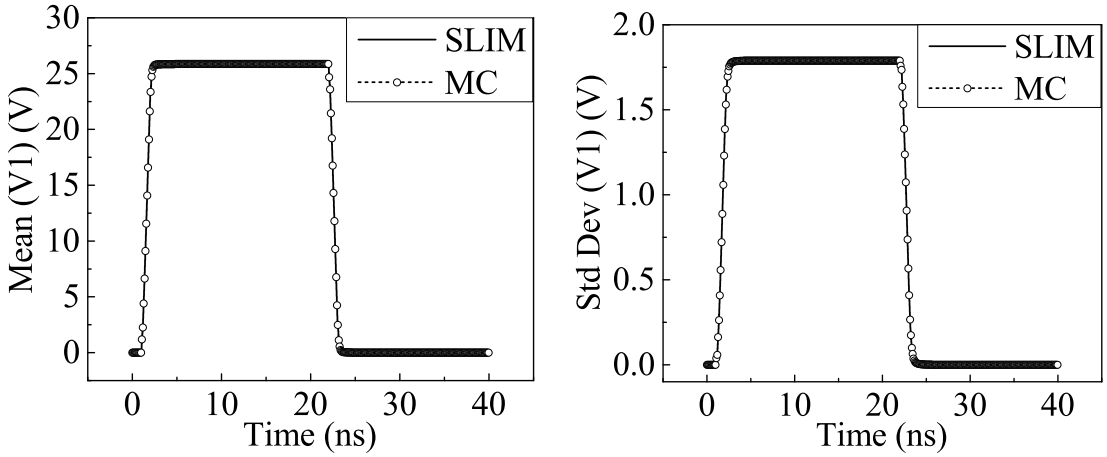

(a) $\mathbb{E}[V1]$

(b) $\mathbb{E}[V4]$

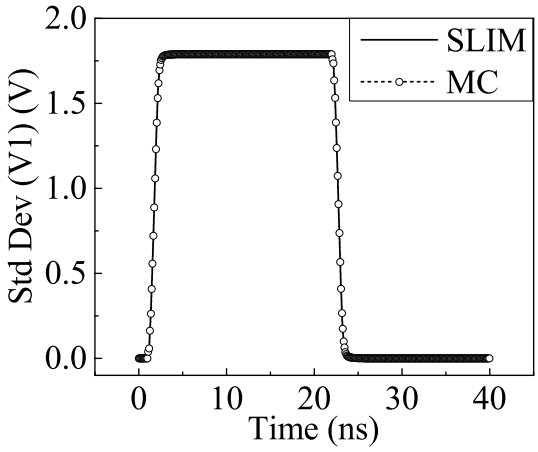

(c) $\sigma(V1)$

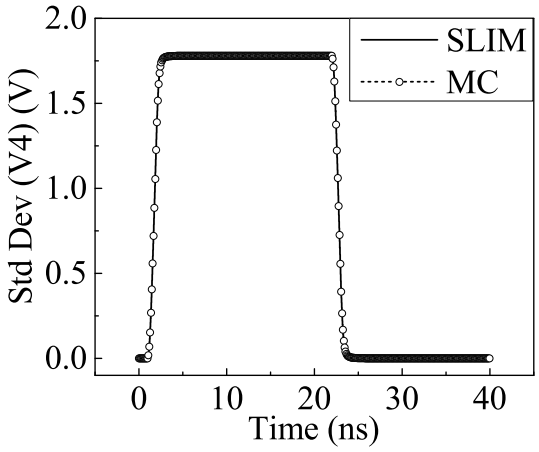

(d) $\sigma(V4)$

Figure 3.4: Stochastic LIM vs. Monte Carlo results for example shown in Figure 3.2 with scaling factor $s = 0.1$. With low latencies, the circuit is almost entirely resistive.

$t \in \mathbb{T}$, the set of discrete time steps. The solution at each node of the sparse grid is used to construct a Lagrange interpolant:

$$\tilde{f}_t(Z) = \sum_{i=1}^{M} Y_{i,t} L_i(Z) \tag{3.25}$$

$$L_i(Z_j) = \delta_{ij} \tag{3.26}$$

The interpolant $\tilde{f}_t(\cdot)$ is an estimate of the actual response $f_t(\cdot)$, but it is much faster to evaluate than the underlying solver. Therefore, we perform Monte Carlo using the interpolant $\tilde{f}_t$, and calculate the statistics as we did in (3.1) and (3.2).

It should be noted that this procedure must be repeated for every element of the set $\mathbb{T}$. In other words, the interpolation and calculation of statistics take place at each time step of the simulation. Since each node corresponds to a deterministic LIM simulation, the stability criterion can be calculated using $\Delta t \leq \sqrt{LC}$ for each simulation. For ease of implementation, it is good to use the same Δt and hence the same set $\mathbb{T}$ for all simulations.

A workflow for the Stochastic Collocation approach to LIM is shown in Figure 3.5.

3.5 Stability Conditions

The stability of the algorithm is conditional on the size of the time step chosen. Generally, the most conservative approach is to let $\Delta t \leq \sqrt{LC}$ where L and C are the smallest inductance and capacitance in the circuit, respectively. However, when running Stochastic LIM with SGM, the simulation may become unstable even if this criterion is met. This occurs when the variance of one of the random variables is set very high. The more rigorous derivation of the stability condition for block LIM [34] can be derived using the amplification matrix $\mathbf{A}$, defined as:

$$\mathbf{A} = \begin{bmatrix} \mathbf{A}_{11} & \mathbf{A}_{12} \\ \mathbf{A}_{21} & \mathbf{A}_{22} \end{bmatrix} = \begin{bmatrix} \mathbf{P}_+\mathbf{P}_- & -\mathbf{P}_+\mathbf{M} \\ \mathbf{Q}_+\mathbf{M}^T\mathbf{P}_+\mathbf{P}_- & \mathbf{Q}_+\mathbf{Q}_- - \mathbf{Q}_+\mathbf{M}^T\mathbf{P}_+\mathbf{M} \end{bmatrix} \tag{3.27}$$

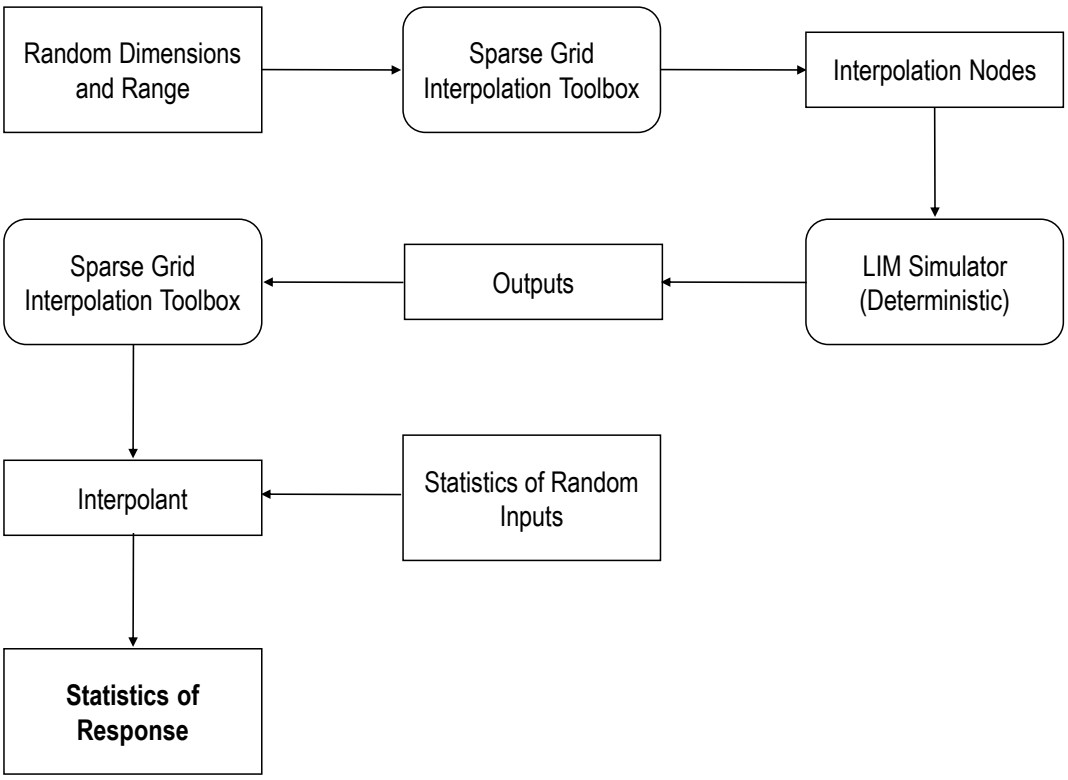

Figure 3.5: Workflow for Stochastic Collocation approach to random simulations with LIM.

where

$$\begin{bmatrix} \mathbf{v}^{n+\frac{1}{2}} \\ \mathbf{i}^{n+1} \end{bmatrix} = \mathbf{A} \begin{bmatrix} \mathbf{v}^{n-\frac{1}{2}} \\ \mathbf{i}^{n} \end{bmatrix}$$

$$\mathbf{P}_{+} = \left(\frac{\mathbf{C}}{\Delta t} + \frac{\mathbf{G}}{2} \right)^{-1} \tag{3.28}$$

$$\mathbf{P}_{-} = \left(\frac{\mathbf{C}}{\Delta t} - \frac{\mathbf{G}}{2} \right) \tag{3.29}$$

$$\mathbf{Q}_{+} = \left(\frac{\mathbf{L}}{\Delta t} + \frac{\mathbf{R}}{2} \right)^{-1} \tag{3.30}$$

$$\mathbf{Q}_{-} = \left(\frac{\mathbf{L}}{\Delta t} - \frac{\mathbf{R}}{2} \right) \tag{3.31}$$

Here we take $\mathbf{R}, \mathbf{L}, \mathbf{G}, \mathbf{C}$ to be the matrices defined in (3.7), (3.8), (3.9) and (3.10), and we can let $\mathbf{M}$ be the identity matrix of dimension P in this case. The time step Δt must be chosen such that the spectral radius of the amplification matrix $\mathbf{A}$ is less than 1. The amplification matrix $\mathbf{A}$ and its eigenvalues will depend on the step size, and it generally will increase with larger Δt, hence a sufficiently small Δt must be chosen to ensure stability of the simulation. Stability is not the only consideration when choosing time step size. Depending on the rate of change of the signal, the time step also should be chosen such that the signal can be properly resolved and sampled.

3.6 Conclusions

Stochastic LIM is demonstrated to be a fast and accurate method for simulating circuits with uncertainties. The formulation presented in this chapter demonstrates that SGM can be implemented easily, effectively, and efficiently with finite difference schemes such as LIM. Like many other stochastic numerical techniques, SGM suffers from the curse of dimensionality, as the terms of polynomial expansion will in-

crease exponentially with the dimensionality of random space. The Stochastic LIM formulation presented here incorporates four random dimensions, and can enable simulations of many practical signal integrity applications such as lossy transmission lines and IC PVT variations. Dimensionality reduction techniques such as Principle Component Analysis (PCA) [5] can also be incorporated with Stochastic LIM to solve higher dimensional problems. This chapter demonstrates that Stochastic LIM can also be implemented using SC together with the deterministic formulation. In the next chapter, we present simulation results using the methodologies presented to study single- and multi-conductor transmission lines.

CHAPTER 4

SIMULATION OF TRANSMISSION LINES WITH UNCERTAINTIES

4.1 Sampling-based EM Extraction

The inputs to the stochastic transmission line (TL) simulation are the physical parameters with uncertainties that are present in the transmission line. The probability distributions of these parameters need to be defined. In this application, the random parameters are generally either Gaussian or uniformly distributed. Uncertainties in these physical TL parameters will manifest in uncertainties of the TL electrical parameters $RLGC$. However, the $RLGC$ parameters will not exhibit any regular Gaussian or uniform distribution. Rather, the electrical parameters will be correlated with each other, and will be dependent on the physical parameters of the line. To characterize the uncertainties of electrical parameters, we must utilize EM field solvers for parameter extraction.

Since many effective commercial and proprietary EM solvers already exist, we will utilize an efficient sampling-based method to construct the stochastic TL model for simulation. The objective of modeling is to extract the gPC expansion coefficients of electrical parameters from geometric parameters with uncertainties. The gPC coefficients can be calculated with polynomial projection:

$$C_{i,k} = \frac{\langle C_i(\omega), \psi_k(\boldsymbol{\xi})\rangle}{\langle \psi_k^2(\boldsymbol{\xi})\rangle} = \frac{1}{\langle \psi_k^2(\boldsymbol{\xi})\rangle} \int_{\mathbb{R}^d} C_i(\boldsymbol{\xi})\psi_k(\boldsymbol{\xi})W(\boldsymbol{\xi})\, d\boldsymbol{\xi} \tag{4.1}$$

This integral needs to be evaluated for each expansion order k and each parameter R, L, G, C etc. Recall that the random parameter $\boldsymbol{\xi}$ characterizes randomness in geometry, hence a closed-form expression for $C_i(\boldsymbol{\xi})$ is usually not available. Therefore,

some sort of discrete sampling method needs to be used to evaluate the integral to calculate the coefficients.

Since $\boldsymbol{\xi}$ is usually multi-dimensional, sparse grid quadrature rules are useful for defining the sampling points where the parameters can be evaluated deterministically using commercially-available solvers, and to calculate the gPC expansion coefficients from the samples. Let $\Theta = \{\boldsymbol{\xi}_i\}_{i=1}^{M_{d,l}}$ be the set of nodes defined by the sparse grid quadrature rule, then the gPC expansion coefficient can be approximated as:

$$C_k \approx \frac{1}{\langle \psi_k^2(\boldsymbol{\xi}) \rangle} \sum_{i=1}^{M_{d,l}} C(\boldsymbol{\xi}_i)\psi(\boldsymbol{\xi}_i)W(\boldsymbol{\xi}_i)w(\boldsymbol{\xi}_i) \tag{4.2}$$

Here $w(\boldsymbol{\xi}_i)$ is the weight associated with each quadrature point. Hence, we only need to perform deterministic EM extractions to calculate the circuit parameter values at the set of pre-defined points Θ to obtain the gPC inputs for Stochastic LIM. Using Smolyak sparse grid quadrature, the number of points needed is approximately:

$$M_{d,l} \approx \frac{2^l d^l}{l!}, \quad \text{for } d \gg 1 \tag{4.3}$$

where $M_{d,l} = |\Theta_{d,l}|$ corresponds to the number of quadrature nodes for random space with dimension d and sparse grid level l.

The quadrature in (4.2) evaluates a definite integral with finite limits, hence it requires that the random space be defined over a finite domain. This is straightforward for random variables with uniform distributions, since these random variables can only take values within a finite region. When calculating expansion coefficients for Gaussian random variables, two complications arise:

1. Gaussian random variables can theoretically take value over the entire real number space. Hence, it is necessary to truncate the random space to a reasonable limit ($\mu \pm 5\sigma$) where it is highly unlikely for the random variables to have value outside of this truncated domain.

2. The Gaussian PDF $W(\boldsymbol{\xi})$ is difficult to integrate accurately with most quadrature rules. A large number of quadrature points are needed, which significantly

increases the computational cost of EM simulations. However, the extracted EM parameters $R(\boldsymbol{\xi}), L(\boldsymbol{\xi}), G(\boldsymbol{\xi}), C(\boldsymbol{\xi})$ are usually smooth functions in the random space, and can be integrated accurately with very few points. Therefore, we propose a two-level multigrid approach to calculating expansion coefficients for Gaussian random variables below.

First, we construct a sparse grid interpolation for the extracted parameter:

$$\tilde{C}(\boldsymbol{\xi}) = \sum_{i=1}^{M_{d,l'}^{L}} \Psi_i^p(\boldsymbol{\xi}_i) C(\boldsymbol{\xi}_i) \tag{4.4}$$

where $\Psi_i^P(\boldsymbol{\xi})$ are Lagrange basis functions of order p used to interpolate the parameter in random space. $M_{d,l'}^{L}$ is the number of nodes needed to construct the interpolation, and corresponds to the number of deterministic EM simulations necessary to interpolate the transmission line parameters. The superscript L denotes that the interpolation nodes are lower in resolution than the quadrature points, i.e. $l' \ll l$. Then, we evaluate the projection integral using a much more dense sparse grid, so the weighting function $W(\boldsymbol{\xi})$ can be integrated accurately:

$$C_k \approx \frac{1}{\langle \psi_k^2(\boldsymbol{\xi}) \rangle} \sum_{i=1}^{M_{d,l}^{H}} \tilde{C}(\boldsymbol{\xi}_i) \psi(\boldsymbol{\xi}_i) W(\boldsymbol{\xi}_i) w(\boldsymbol{\xi}_i) \tag{4.5}$$

Here we substitute in the interpolation $\tilde{C}(\boldsymbol{\xi})$ in the integrand, which is very fast to evaluate when compared to full deterministic simulations. $M_{d,l}^{H}$ is the number of points needed to construct the high-resolution quadrature.

It is worth noting that the integral (4.1) does not necessarily have to be evaluated with a deterministic quadrature rule. In fact, the coefficients can also be recovered from Monte Carlo integration. This means that if the probability distributions of the random parameters are not known, but a large sample size is available, the gPC coefficients can be calculated from repeated measurements of the samples without knowing the closed-form PDF of random parameters. This will also allow stochastic models to be constructed from hardware measurements.

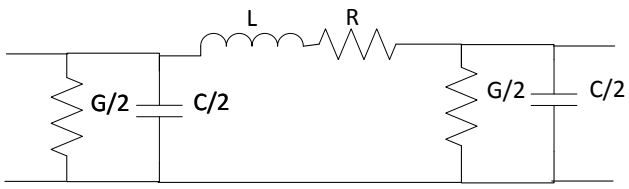

Figure 4.1: Lumped single-line transmission line circuit in $\pi-$topology.

4.2 Lumped Transmission Line Model

Stochastic LIM has been used in [41] and [42] to simulate single transmission lines with random p.u.l. R, L, G, C parameters using the $\pi-$topology shown in Figure 4.1. However, modifications to the original LIM procedure are needed to simulate coupled transmission lines, since mutual inductance between branches and mutual capacitance between nodes need to be accounted for. In [43], a fictitious inductance is inserted in series with mutual capacitance to introduce latency and allow for stable simulation. However, this technique introduces some inaccuracies into the circuit. Thus, we use the technique introduced in [44] to incorporate mutual reactances for coupled transmission line models.

The coupled transmission line is modeled as a $\pi-$model, as shown in Figure 4.2. Each end of the line segment is considered a coupled supernode. The coupled nodal capacitance is written in Maxwellian matrix form

$$\bar{\mathbf{C}} = \begin{bmatrix} [\mathbf{C_{11}}] & [\mathbf{C_{12}}] \\ [\mathbf{C_{21}}] & [\mathbf{C_{22}}] \end{bmatrix} = \begin{bmatrix} [\mathbf{C_s} + \mathbf{C_m}] & [-\mathbf{C_m}] \\ [-\mathbf{C_m}] & [\mathbf{C_s} + \mathbf{C_m}] \end{bmatrix} \tag{4.6}$$

and coupled branch inductance for a superbranch is:

$$\bar{\mathbf{L}} = \begin{bmatrix} [\mathbf{L_s}] & [\mathbf{L_m}] \\ [\mathbf{L_m}] & [\mathbf{L_s}] \end{bmatrix} \tag{4.7}$$

Here the self and mutual capacitance and inductance matrices come from the gPC expansion in (3.19) and (3.23). A supernode should contain all nodes that have

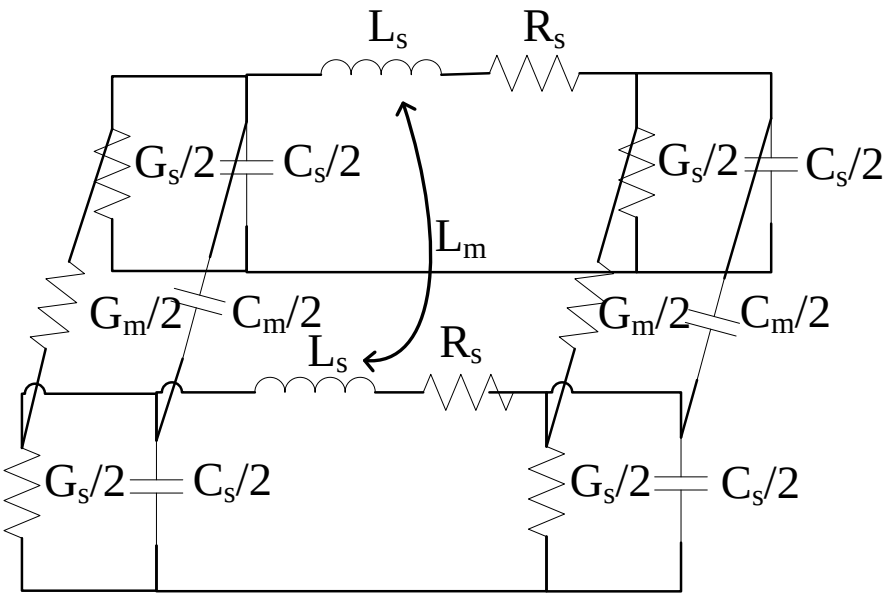

Figure 4.2: Lumped $\pi-$model for coupled transmission line.

mutual capacitances with each other, and a superbranch should contain all branches that have mutual inductances with each other. This approach could slow down LIM for problems where an arbitrarily large number of nodes and branches share mutual reactances, but in the case of multi-conductor transmission lines, the computational complexity still scales linearly with respect to the size of the circuit.

To keep track of node connectivity and direction of current flow in the $\pi-$topology, we can take advantage of connectivity matrix $\mathbf{M}$ of size $N_n \times N_b$, where N_n is the number of supernodes and N_b is the number of superbranches. In this topology,

$$\sum_{j=1}^{M_i} \mathbf{I}_{ij}^n = [\mathbf{M}\mathbf{I}^n]_{(\cdot,i)}^T \tag{4.9}$$

$$\mathbf{I}^n = \begin{bmatrix} I_{12,0,a}^n & I_{12,1,a}^n & \cdots & I_{12,P,a}^n & I_{12,0,b}^n & I_{12,1,b}^n & \cdots & I_{12,P,b}^n \\ I_{23,0,a}^n & I_{23,1,a}^n & \cdots & I_{23,P,a}^n & I_{23,0,b}^n & I_{23,1,b}^n & \cdots & I_{23,P,b}^n \\ \vdots & \vdots & \cdots & \vdots & \vdots & \vdots & \cdots & \vdots \\ I_{N_bN_n,0,a}^n & I_{N_bN_n,1,a}^n & \cdots & I_{N_bN_n,P,a}^n & I_{N_bN_n,0,b}^n & I_{N_bN_n,1,b}^n & \cdots & I_{N_bN_n,P,b}^n \end{bmatrix} \tag{4.10}$$

$$\mathbf{V}_i^{n+\frac{1}{2}} - \mathbf{V}_j^{n+\frac{1}{2}} = \left[\mathbf{M}^T\mathbf{V}^{n+\frac{1}{2}}\right]_{(\cdot,i)}^T \tag{4.11}$$

$$\mathbf{V}^{n+\frac{1}{2}} = \begin{bmatrix} V_{1,0,a}^{n+\frac{1}{2}} & V_{1,1,a}^{n+\frac{1}{2}} & \cdots & V_{1,P,a}^{n+\frac{1}{2}} & V_{1,0,b}^{n+\frac{1}{2}} & V_{1,1,b}^{n+\frac{1}{2}} & \cdots & V_{1,P,b}^{n+\frac{1}{2}} \\ V_{2,0,a}^{n+\frac{1}{2}} & V_{2,1,a}^{n+\frac{1}{2}} & \cdots & V_{2,P,a}^{n+\frac{1}{2}} & V_{2,0,b}^{n+\frac{1}{2}} & V_{2,1,b}^{n+\frac{1}{2}} & \cdots & V_{2,P,b}^{n+\frac{1}{2}} \\ \vdots & \vdots & \cdots & \vdots & \vdots & \vdots & \cdots & \vdots \\ V_{N_n,0,a}^{n+\frac{1}{2}} & V_{N_n,1,a}^{n+\frac{1}{2}} & \cdots & V_{N_n,P,a}^{n+\frac{1}{2}} & V_{N_n,0,b}^{n+\frac{1}{2}} & V_{N_n,1,b}^{n+\frac{1}{2}} & \cdots & V_{N_n,P,b}^{n+\frac{1}{2}} \end{bmatrix} \tag{4.12}$$

$N_n = N_b + 1$, and the connectivity matrix is:

$$\mathbf{M} = \begin{bmatrix} 1 & 0 & 0 & \cdots & 0 \\ -1 & 1 & \ddots & \ddots & \vdots \\ 0 & -1 & \ddots & \ddots & \vdots \\ \vdots & \ddots & \ddots & 1 & 0 \\ \vdots & 0 & \ddots & -1 & 1 \\ 0 & 0 & 0 & 0 & -1 \end{bmatrix} \tag{4.8}$$

where $M_{i,i} = 1$ and $M_{i+1,i} = -1$, $\forall i \in \{1, 2, ..., N_b\}$. The current and voltage summation terms in (3.15) and (3.22) can be simplified using equations (4.9)-(4.12), where the subscript $(\cdot, i)$ denotes the $i-$th column of the matrix, and the subscript a and b in the gPC coefficients denote voltage and currents associated with conductors a and b, respectively. During post-processing to calculate statistics, the values on each conductor should be calculated separately using (3.24).

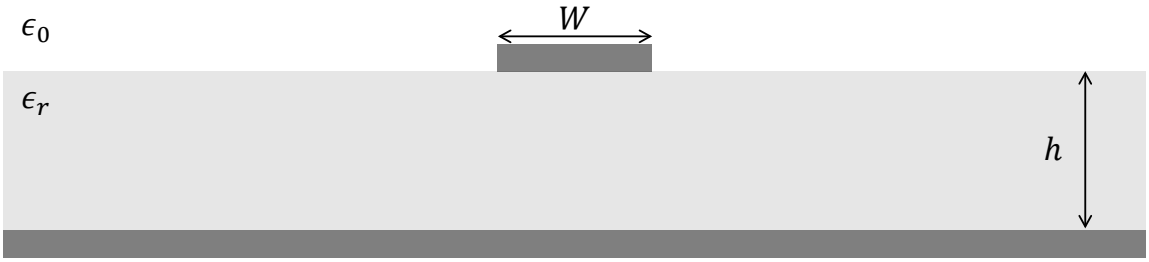

Figure 4.3: Cross-section of the single microstrip line model. The random parameters in this model are dielectric constant ϵ_r, substrate thickness h, and line width W, each with an independent Gaussian distribution.

4.3 Numerical Examples

4.3.1 Single Microstrip Line with Geometric Uncertainties

The first example is a single microstrip line of length $L = 50\,\text{cm}$ where the geometry and substrate property are random. As shown in Figure 4.3, the width of the trace W, the thickness of the dielectric substrate h, and the dielectric constant of the substrate ϵ_r are independent Gaussian random variables. The variation in ϵ_r and thickness h can result from inaccuracies in material construction, and ϵ_r can vary as a result of inaccurate fiber-resin ratio or the fiber-weave effect, which will be investigated in a later example. The width can have variability from the design value depending on the etching process. For instance, longer than desired exposure time to etchant would cause the line to be narrower than designed, and vice versa.

The random parameters for this example are summarized in Table 4.1. A stochastic model for the transmission line is constructed using sparse grid sampling, with 3 random dimensions and interpolation level $l' = 4$, which corresponds to 177 deterministic simulations with EM extractor. The line is driven with a trapezoidal pulse voltage source shown in Figure 4.4 with source impedance $50\,\Omega$, and is terminated with a load impedance of $50\,\Omega$. The voltage at the input (V_{in}) and output (V_{out}) of the line are measured, as demonstrated in Figure 4.5.

The results from Stochastic LIM are compared to a Monte Carlo (MC) simulation

Table 4.1: Random parameters for single microstrip line with geometric uncertainties.

Parameter	Distribution
W	$\mathcal{N}(0.1, 0.01)$ mm
h	$\mathcal{N}(0.2, 0.02)$ mm
ϵ_r	$\mathcal{N}(4.4,0.44)$

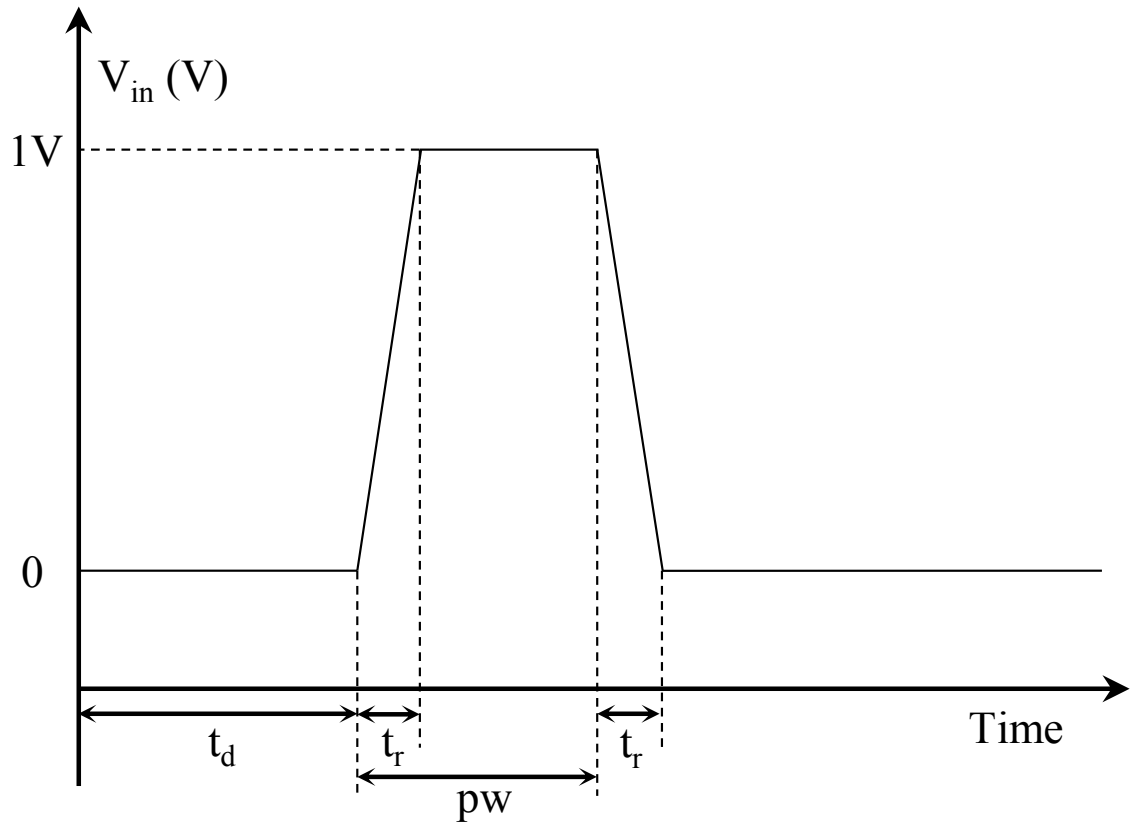

Figure 4.4: The excitation function V_{in}. For this simulation, $t_d = 1$ ns, $t_r = 500$ ps, $pw = 20$ ns.

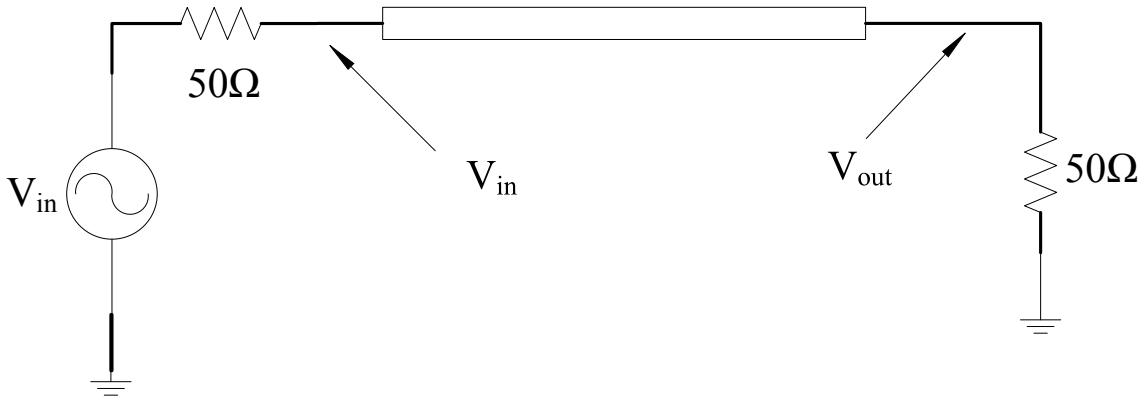

Figure 4.5: Simulation setup for single-line pulse excitation simulation over microstrip line.

using a commercial circuit solver. To perform the MC simulation, 1000 samples of the input parameters (W, h, ϵ_r) are generated according to their probability distribution, a model is generated using EM extractor for each sample, and a deterministic circuit simulation is performed for each model. All 1000 time series results are saved and post-processed to obtain the statistics. In Figure 4.6, 21 of the deterministic results are plotted along with the statistical results generated from Stochastic LIM. We can see that the Stochastic LIM results, represented by the shaded area, encapsulate all the deterministic results. For a closer look at the accuracy of Stochastic LIM, we compare the standard deviation of the probed voltages as calculated by Stochastic LIM vs. MC in Figure 4.7, and we can see that the statistics generated by both methods compare very well. The total simulation times of both methods are summarized in Section 4.4.

4.3.2 Coupled Microstrip Line with Geometric Uncertainties

We simulate a coupled microstrip of length $L = 50\,\text{cm}$ on a homogeneous PCB substrate to demonstrate that Stochastic LIM can simulate multi-conductor transmission lines and characterize the uncertainties in crosstalk measurements. The cross-section is shown in Figure 4.8, and the random parameters are the edge-to-edge spacing s,

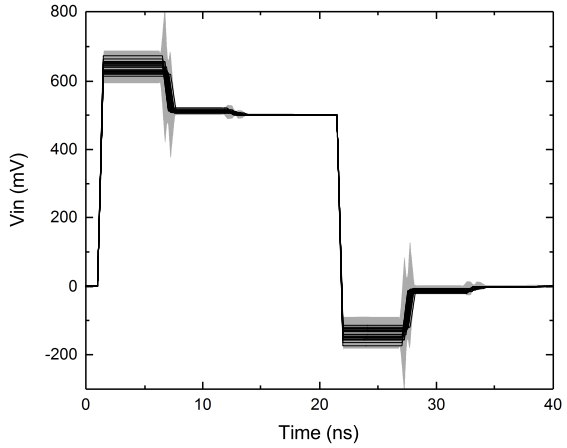

(a) V_{in} (Near-end)

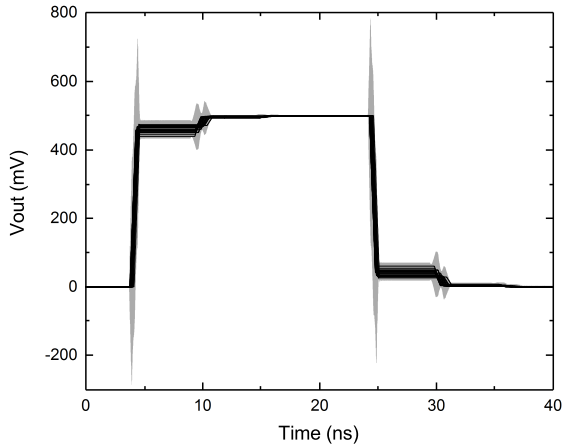

(b) V_{out} (Far-end)

Figure 4.6: Voltages at near-end and far-end of single-line microstrip with geometric and material uncertainties. Shaded region represents the mean response $\pm 3\sigma$ as calculated by Stochastic LIM. The solid lines represent 21 deterministic simulations using Ansys Nexxim simulator.

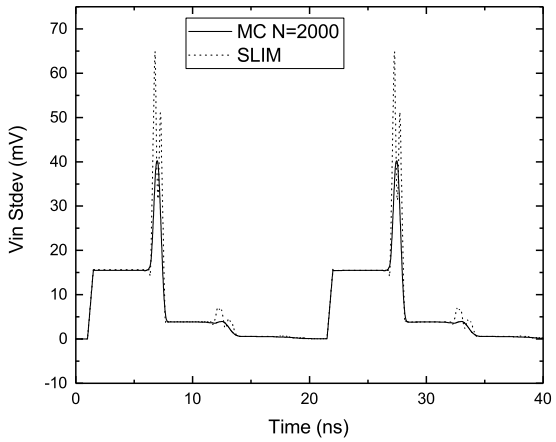

(a) σ_{Vin} (Near-end)

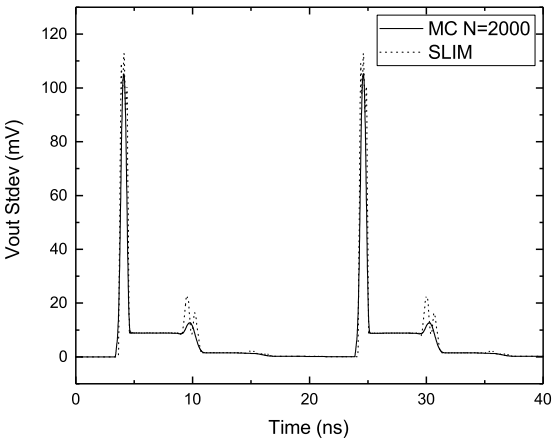

(b) σ_{Vout} (Far-end)

Figure 4.7: Standard deviation σ of near- and far-end voltage on single-line microstrip with geometric uncertainties as calculated by Monte Carlo $N = 2000$ and Stochastic LIM.

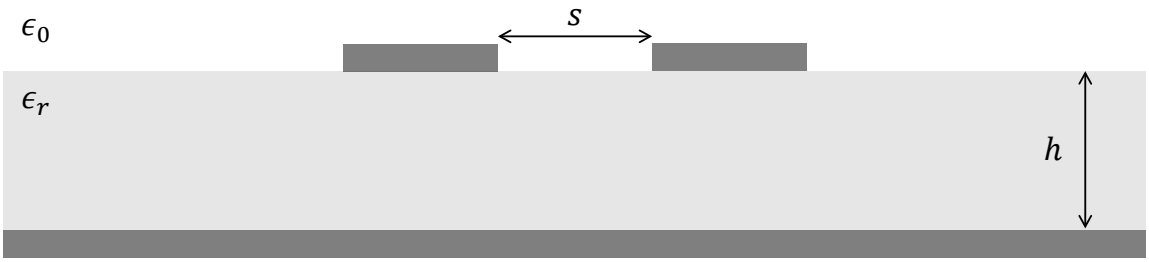

Figure 4.8: Cross-section of coupled microstrip line. The random parameters in this model are substrate dielectric constant ϵ_r, substrate thickness h, and edge-to-edge spacing s, each with an independent Gaussian distribution.

Table 4.2: Random parameters for coupled microstrip line with geometric uncertainties.

Parameter	Distribution
s	$\mathcal{N}(0.1, 0.003)$ mm
h	$\mathcal{N}(0.2, 0.005)$ mm
ϵ_r	$\mathcal{N}$(4.4,0.1)

the thickness of dielectric substrate h, and the dielectric constant ϵ_r. The probability distributions of the parameters are summarized in Table 4.2. The simulation circuit is shown in Figure 4.9. The aggressor line is connected to a pulse voltage source with source impedance $50\,\Omega$, driving the trapezoidal source shown in Figure 4.4, and terminated with $50\,\Omega$. The victim line is terminated on both ends with $50\,\Omega$ loads. The near-end crosstalk (NEXT) and far-end crosstalk (FEXT) are measured at the two ends of the victim line. This example also has 3 random dimensions and we use a sparse grid with interpolation level $l' = 4$, resulting in 177 deterministic EM extractor simulations needed to obtain the stochastic model.

The results are compared to MC simulation of 1000 samples performed using a commercially available deterministic solver. In Figures 4.10 we can see the statistics calculated by Stochastic LIM as the shaded area, along with results from 21 deterministic simulations. In Figure 4.11, the standard deviations of NEXT in time as calculated by Stochastic LIM and MC are compared and show very good agreement.

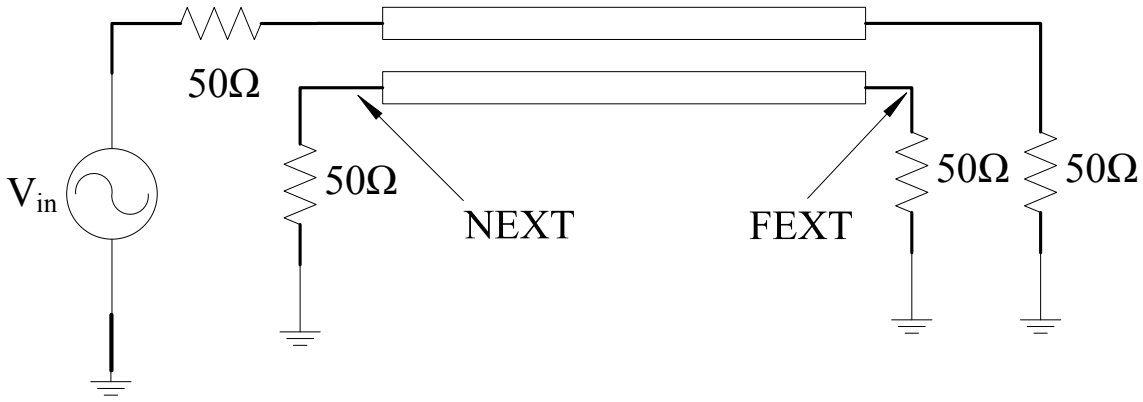

Figure 4.9: Simulation setup for crosstalk simulation over coupled microstrip line.

Figures 4.12 and 4.13 show the same data for FEXT.

4.3.3 Coupled Microstrip Line with Fiber-Weave Effect

High-speed links are ubiquitous in computer system design. Most of the modern high-speed links utilize differential signaling, which relies on the voltage difference between two signal conductors to transmit waveforms. For high-speed links that include printed circuit board (PCB) traces as part of the channel, the differential signal is prone to degradation from the fiber-weave effect, which results from the inhomogeneous electrical properties of glass fiber and epoxy resin substrates that are typically used for PCBs. In [9], it was shown that the extent of signal degradation resulting from fiber-weave effect is dependent on the relative position of the etched traces with respect to the glass fiber bundles in the substrate. Since this relative position cannot be controlled during etching, its exact value is uncertain and hence the effects are best modeled using stochastic techniques. In this chapter, we use the Stochastic LIM technique introduced in [45] to study the fiber-weave effect. A method of using existing commercial EM solvers to obtain the necessary input parameters for Stochastic LIM is also shown.

We simulate a segment of transmission line with fiber-weave effect. The differential microstrip line is 50 cm long, with copper thickness of 0.015 mm and substrate

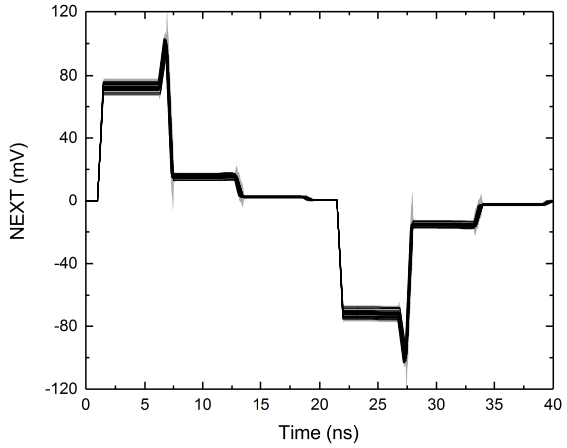

(a) $t \in [0, 40]$ ns

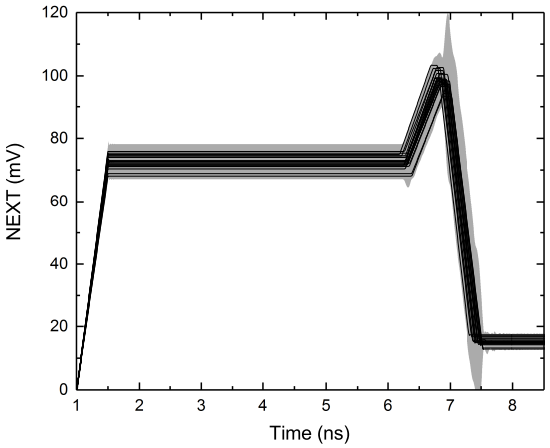

(b) Zoom in to $t \in [1, 8.5]$ ns

Figure 4.10: Near-end crosstalk (NEXT) results of coupled transmission line simulation. Shaded region represents the mean response $\pm 3\sigma$ as calculated by Stochastic LIM. The solid lines represent 21 deterministic simulations using Ansys Nexxim simulator.

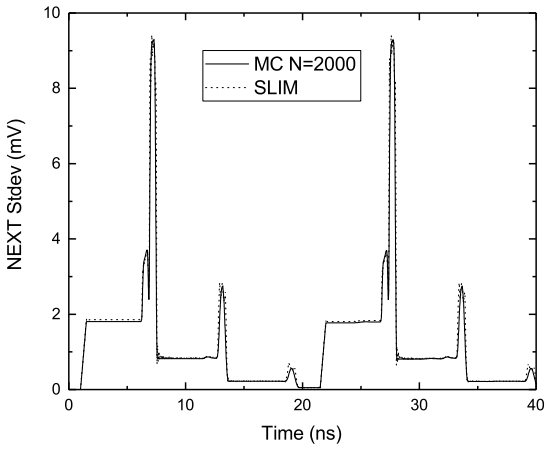

(a) $t \in [0, 40]$ ns

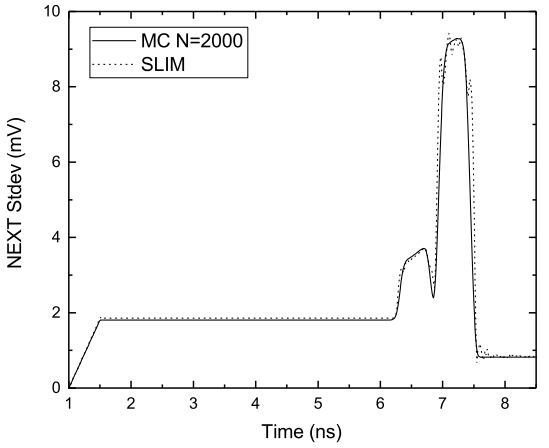

(b) Zoom in to $t \in [1, 8.5]$ ns

Figure 4.11: Standard deviation σ of NEXT as calculated by Monte Carlo $N = 2000$ and Stochastic LIM.

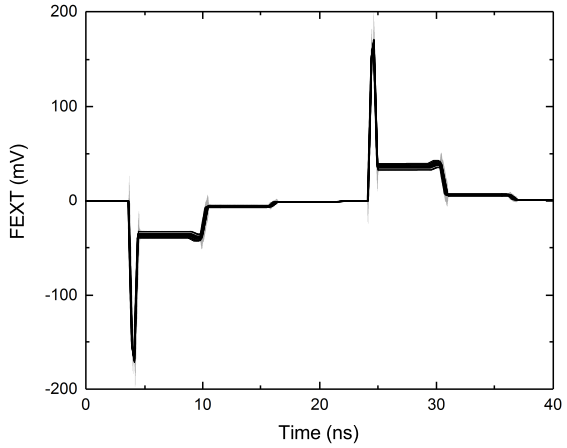

(a) $t \in [0, 40]$ ns

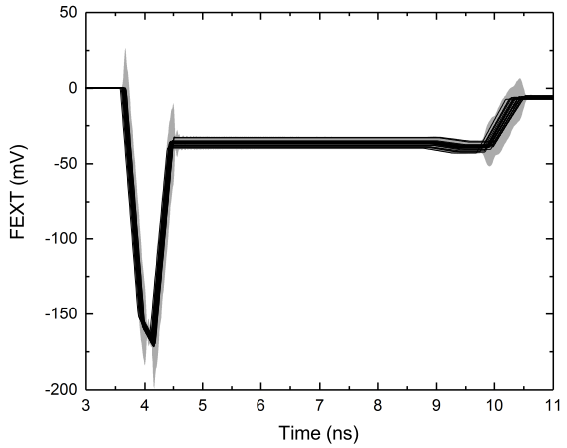

(b) Zoom in to $t \in [3, 11]$ ns

Figure 4.12: Far-end crosstalk results of coupled transmission line simulation. Shaded region represents the mean response $\pm 3\sigma$ as calculated by Stochastic LIM. The solid lines represent 21 deterministic simulations using Ansys Nexxim simulator.

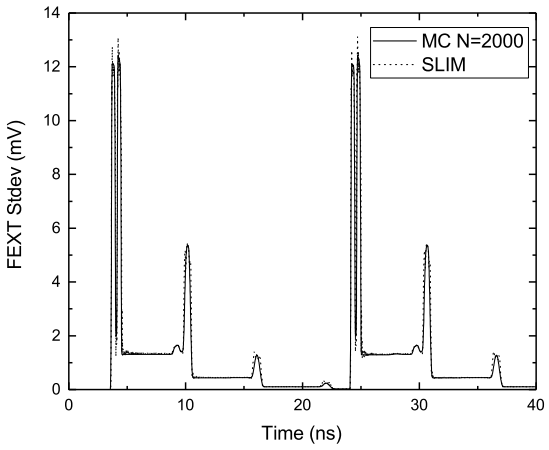

(a) $t \in [0, 40]$ ns

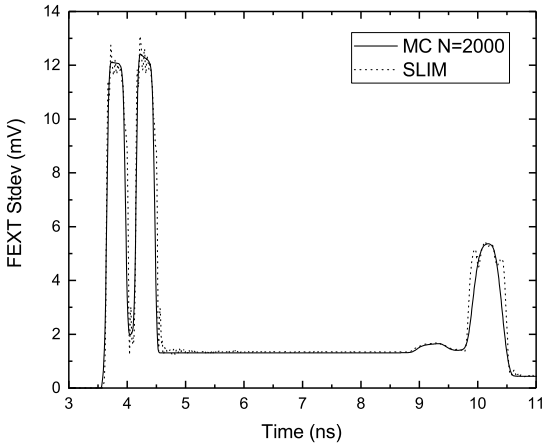

(b) Zoom in to $t \in [3, 11]$ ns

Figure 4.13: Standard deviation σ of FEXT as calculated by Monte Carlo $N = 2000$ and Stochastic LIM.

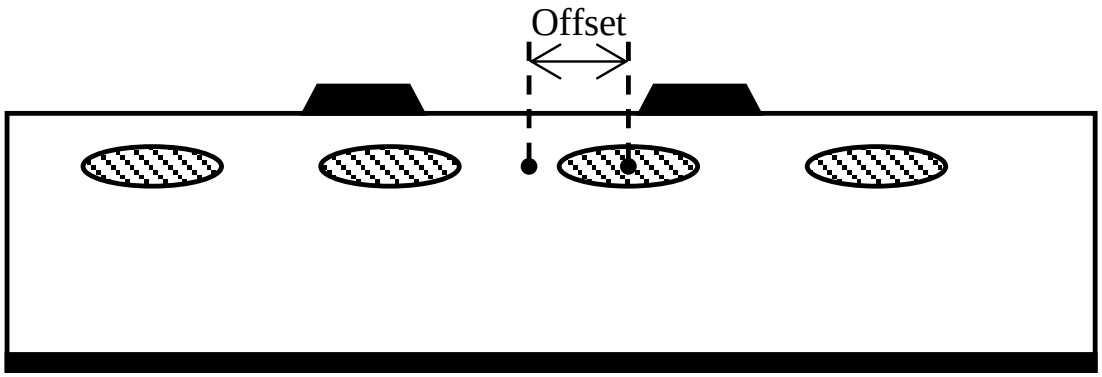

Figure 4.14: Cross-section of coupled microstrip line with fiber bundles.

thickness of 0.2 mm. The pair of microstrips has width of 0.1 mm and edge-to-edge spacing of 0.1 mm. The fiber bundles in the substrate are represented by oval cylinders with dielectric constant. The relative position of the microstrip pair with respect to the fiber bundles is represented by a uniformly distributed random variable "offset" as shown in Figure 4.14, taking the distribution $offset \sim \mathcal{U}(-0.175\,\text{mm}, 0.175\,\text{mm})$. This variable is uniformly distributed since the positions of the fiber bundles are not calibrated during fabrication, and it is equally likely to take on any value within the range. As shown in Figure 4.15, the transmission line pair is driven with a differential clock signal with $V_{low} = -1.2\,\text{V}$ and $V_{high} = 1.2\,\text{V}$, at a rate of 2 Gbps and rise/fall time of 200 ps. The far-ends of both lines are terminated with $50\,\Omega$ resistors. The driver impedance is $100\,\Omega$.

The near-end and far-end differential voltages are shown in Figure 4.16. The solid lines represent deterministic simulations performed with ANSYS Nexxim circuit simulator, while the shaded area represents the mean $\pm 2\sigma$ of the statistics calculated from Stochastic LIM. As can be seen, the results from Stochastic LIM encapsulate the results from deterministic simulations very well.

Since this problem has only one random dimension, we expand it using Legendre polynomial and a sparse grid of dimension 1 and level $l' = 4$, resulting in only 21 deterministic solutions with the EM extractor needed to construct the stochastic model.

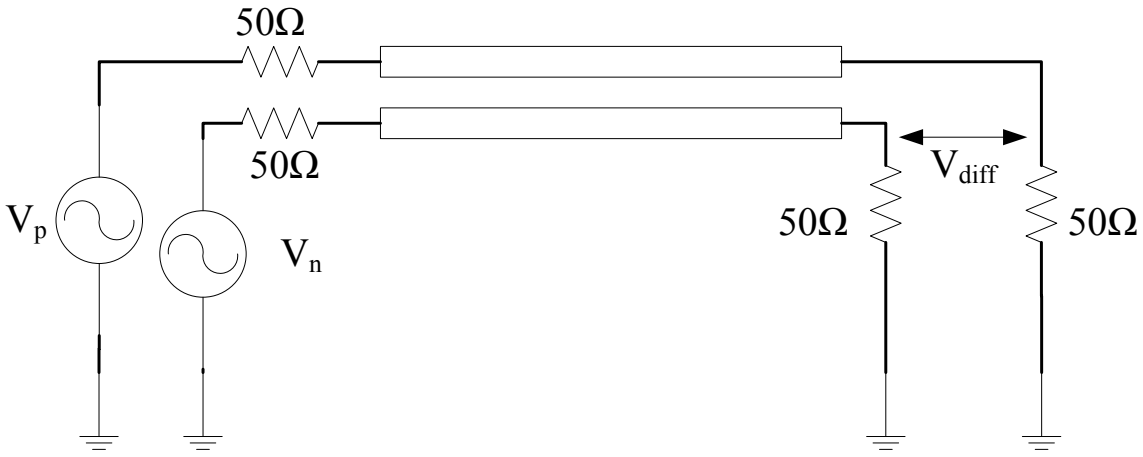

Figure 4.15: Differential signal simulation setup. The signals V_p and V_n are complementary clock signals operating at 2 Gbps, with $t_r = t_f = 200\,\text{ps}$.

4.4 Benchmark and Conclusions

4.4.1 Computational Efficiency

The computational times of the three examples presented in this chapter are summarized in Tables 4.3 and 4.4. The speed-up of the Stochastic LIM workflow is a result of two advancements. First, the number of expensive EM extractor runs is minimized by utilizing sparse grid quadrature techniques to recover the gPC expansion coefficients of transmission line parameters. In Monte Carlo analysis, a deterministic EM simulation is required for each randomly drawn sample of input parameters, which is very expensive. It should be noted that both the proposed EM modeling technique and Monte Carlo utilize existing deterministic solvers and operate on input points that are defined a-priori. Thus the solution of each instance can be easily accelerated with parallel computing in both methods.

The second source of speed-up is the SGM formulation of LIM. By solving the transient simulation using the proposed technique, only a single simulation of an expanded state-space system is necessary. For MC, or any sampling-based methodology for that matter, multiple instances of transient circuit simulation will be necessary.

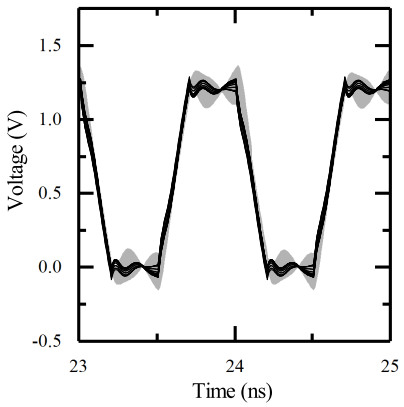

(a) Near-end

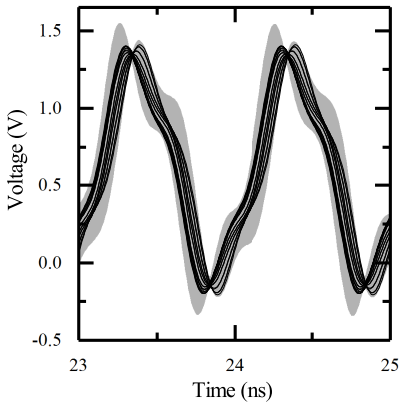

(b) Far-end

Figure 4.16: Differential voltage measured at the input and output of the coupled transmission line. The shaded areas represent mean voltage $\pm 2\sigma$ as calculated by Stochastic LIM. The black lines represent deterministic solutions calculated using ANSYS Nexxim.

Table 4.3: Computational time comparison of Stochastic LIM implemented in MATLAB vs. Monte Carlo $N = 1000$ with Ansys Nexxim using W-element model. Parallel computing is used for Monte Carlo and EM simulations.

Example	# of EM Simulations	Run Time (sec)	MC $N = 1000$ Run Time (sec)	Speed-up
Single-line	177	1195	4710	**3.9**
Coupled-line	177	1732	5522	**3.2**
Fiber-weave	21	189	6792	**35.9**

Table 4.4: Computational time comparison of Stochastic LIM compiled using C++ vs. Monte Carlo $N = 1000$ simulation with Ansys Nexxim lumped circuit model. Parallel computing over 3 cores is used for Monte Carlo and EM simulations.

Example	EM Extraction (sec)	Transient Simulation (sec)	Post-Processing (sec)	Total (sec)	Speed-up
Coupled-line (SLIM)	402	107	10	519	**48.02505**
Coupled-line (MC)	3990	14000	6935	24925	
Fiber-weave (SLIM)	49	41	10	100	**292.02**
Fiber-weave (MC)	5011	14000	10191	29202	

Although the computational time of the sampling techniques can be mitigated by utilizing parallel computing resources, the amounts of data generated for transient simulations are typically massive. Furthermore, extensive post-processing will be necessary to parse through all the deterministic circuit simulation results to gather the statistics in time domain. With Stochastic LIM, only the gPC expansion coefficients of quantities of interest are outputted, which can quickly be translated into statistical quantities of interest without the need to process large amounts of data.

The performance benchmarks presented here are performed on a Dell Precision T5600 workstation with 6-core Intel Xeon E5-2630 CPU at 2.3 GHz clock speed, and 32 GB of memory. Parallel simulations are utilized in EM extraction and circuit simulation whenever possible. The Stochastic LIM simulation is implemented in MATLAB.

For the last two examples, Stochastic LIM was converted from MATLAB native to C++ compiled, which offered significant speed-up of run-time. This is demonstrated in Table 4.4.

4.4.2 Data Storage Efficiency

An attractive feature of performing transient analysis using intrusive solver is that only the gPC expansion coefficients need to be stored and post-processed. Any non-intrusive sampling techniques, including MC and SC, require that entire time series corresponding to each sample be stored for post-processing. This can lead to very large data storage requirements. For instance, in the coupled line example problem shown, the transient solutions for all $N = 1000$ runs are stored for $t \in [0, 40]ns$ in $\Delta t = 1ps$ steps, and the total storage is 632 MB. The large amount of data also increased the time needed for post-processing to obtain statistics, which was 6935 seconds. The results from Stochastic LIM for the same problem only needed to have the 15 gPC expansion coefficients stored in time. This leads to a file of only 2.5 MB and post-processing took less than 10 seconds. The comparison of data storage requirement for Stochastic LIM and Monte Carlo is shown in Table 4.5.

Table 4.5: Data storage and post-processing requirements for coupled line and fiber-weave examples. Monte Carlo results correspond to $N = 1000$ runs using Ansys Nexxim.

Example	Data Size (SLIM)	Post-Processing Time (SLIM)	Data Size (MC)	Post-Processing Time (SLIM)
Coupled-line	2.5 MB	10 sec	632 MB	6935 sec
Fiber-weave	1.3 MB	10 sec	827 MB	10191 sec

4.4.3 Conclusions

In this chapter, a complete modeling-to-simulation methodology based on Stochastic LIM for transmission lines with uncertainties is presented. The efficiency and accuracy of the proposed methodology are compared with currently commercially available software for simulating several configurations of microstrip transmission lines with uncertainties in geometric parameters and material uncertainties. The method utilizes existing EM solvers to obtain a stochastic model for the transmission lines, and uses a very efficient time-domain simulator to obtain time-domain voltage and current solutions. We demonstrated that the transmitted signal, near- and far-end crosstalk, and effects of fiber-weave effect can be obtained from this technique. It is demonstrated that the proposed technique can have orders of magnitude improvement in run time and data storage requirements over Monte Carlo simulation using SPICE. The intrusive algorithm proposed in the preceding chapter is an appropriate method to solve well-defined and easily-reformulated cases such as transmission lines. However, sometimes the system under study is very complicated and may involve multiple levels of physical and circuit solutions. For certain parts of the problem, efficient and powerful tools already exist, and thus reformulation using SGM may not be the optimal approach. In the next chapter, some problems of this sort are studied using non-intrusive Stochastic Collocation techniques.

CHAPTER 5

STOCHASTIC SIMULATION OF MULTI-LEVEL AND RESONANT SYSTEMS

5.1 Non-intrusive Stochastic Collocation Approach

In recent years, various fast stochastic numerical techniques [46] have been utilized to solve various electromagnetic [5, 21] and circuit [45, 3, 22, 1, 8, 23, 7] problems where uncertainties in the input parameters require that the output parameters be characterized in the probability domain. Stochastic numerical techniques can be classified into intrusive and non-intrusive types. Intrusive methods require that the governing equations be re-derived and code be re-implemented to leverage the expansion of random variables using orthogonal basis functions. These methods have been widely used [45, 1, 8] for problems where the underlying code is relatively simple to implement, and are very effective as shown in Chapters 3 and 4.

The non-intrusive methods use existing numerical solvers to obtain solutions to deterministic instantiation of the stochastic problem, and calculate the probability information based on the deterministic sample solutions. The most widely utilized non-intrusive method is Monte Carlo (MC) sampling, where the statistical moments are calculated from samples of input parameters drawn from random space, based on their respective probability distributions. Stochastic Collocation (SC) is an often-used sampling technique [20] that converges faster than MC, although this advantage may be lost when the dimensionality of the random space is high ($d > 10$). SC first constructs an interpolation to estimate the output parameters in random space, then calculates the statistical moments and density functions via MC sampling of the interpolation. The speed-up comes from the fact that the interpolation is much

faster to evaluate compared to the actual output. The procedure for SC is discussed in Section 2.3.

In this chapter, we demonstrate that the non-intrusive Stochastic Collocation approach is appropriate for problems where effective but complicated solvers already exist. The problem being considered does not need to be limited to a single problem scale. In Sections 5.2 through 5.4, we study a multi-level and multi-scale problem to demonstrate that uncertainties at the macroscopic electromagnetic level can manifest in randomness at the smaller circuit scale.

In Section 5.5, we study a problem exhibiting resonant behavior in random space. Such problems are traditionally challenging to solve using SC since the cost function interpolation can be expensive to construct. We demonstrate that using adaptive sampling with wavelet basis, we are able to accelerate the solution of resonant problems using the SC method.

5.1.1 Black-box Modeling of Large Systems

An advantage of non-intrusive methods is that complicated solvers can be utilized in sampling techniques. Usually, the outputs $f(\vec{x})$ are the solutions of the underlying differential equations governing the problem. But when sampling techniques are used, the outputs are not limited to be solutions to a single numerical solver. This is useful for large, multi-scale and multi-level problems, where various different simulators are used to solve portions of the problem, and the intermediate results are transferred between solvers without involvement from SC. Only the final output from the last step of the process is needed to construct the interpolation. The complicated simulation process and tools can be encapsulated in a "black box", where the nodes $\Theta_{d,k}$ go in, and the results $f(\Theta_{d,k})$ come out.

5.1.2 Sparse Grid Interpolation

To perform fast SC, sparse grids generated using the Smolyak algorithm [40] are often used to minimize the number of collocation nodes where the response needs to

be evaluated, while maintaining an optimal interpolation accuracy. To allow for local mesh refinement in the random space, a piece-wise basis function is used to construct the interpolation. Compared with interpolation schemes that use global polynomial basis functions which span the entire random domain, local basis functions more accurately interpolate non-smooth functions with locally sharp behavior. The output of a system $f(\vec{x})$ is approximated as:

$$\tilde{f}(\vec{x}) = \sum_{i=1}^{M} \psi_i^p(\vec{x}) f(\vec{x}_i) \tag{5.1}$$

where $\psi_i^p(\vec{x})$ are Lagrange basis functions of order p used to interpolate the response in random space. Hence, for a given interpolation, $\tilde{f}(\vec{x}_i) = f(\vec{x}_i)$ at all collocation nodes $\Theta_{d,k} = \{\vec{x}_i\}_{i=1}^{M}$. Elsewhere in the random domain, the function is approximated and thus will have a residual associated with interpolation error. Under the Smolyak scheme, the cardinality $|\Theta_{d,k}| = M_{d,k}$ is determined by the dimensionality d of the random space, as well as the level of interpolation k. For high-dimensional problems, the number of collocation nodes can be approximated:

$$M_{d,k} \approx \frac{2^k d^k}{k!}, \quad \text{for } d \gg 1 \tag{5.2}$$

We note that this number does not grow favorably w.r.t. k, especially for cases where d is high. For example, the numbers of nodes for problems of dimensions $d = \{2, 6\}$ and various levels are listed in Table 5.1. Hence, SC can be highly effective for problems with low and moderate random dimensions, but the payoff decreases if the dimensionality grows too high.

5.2 Multi-level EM and Circuit Simulation

In this section, we consider using non-intrusive SC to model system-level electromagnetic interference (EMI) in a multi-level system. Such problems can be multi-scale in the sense that effects from EMI on a macroscopic scale can affect performance of cir-

Table 5.1: Number of sparse grid nodes for $d = \{2, 6\}$ and $k = \{1, \ldots, 7\}$.

k	$d = 2$		$d = 6$	
	$M_{d,k}$	$M_{d,k} - M_{d,k-1}$	$M_{d,k}$	$M_{d,k} - M_{d,k-1}$
1	5		13	
2	13	8	85	72
3	29	16	389	304
4	65	36	1457	1068
5	145	80	4865	3408
6	321	176	15121	10256
7	705	384	44689	29568

cuitry on a microscopic, or circuit board, scale. This type of analysis faces challenges stemming from excessive complexity due to the multi-scale nature of the problem. Since the geometric scales can differ by orders of magnitude, the EM field interactions between components with vastly different feature sizes are expensive to account for. Typical EM field solvers will need to create meshes at sizes where the smallest features can be resolved, but such meshes cause the solution of the macroscopic scale problem to be intractable. In addition to challenges with numerical solution of such problems, we wish to account for variability in the problem on each scale, and to study the effect of variabilities on macroscopic scales on the performance of the smaller-scale sub-systems.

To address these challenges, we propose a hybrid EM/circuit modeling methodology [47] to enable solution of problems containing multiple electrical size scales. The flow is shown in Figure 5.1.

An example of a multi-level EM and circuit problem we consider is shown in Figure 5.2. In this case, the vehicle is both physically and electrically large, with feature sizes on the order of a wavelength. The vehicle is subject to external EMI radiation, which is random. The radiation is coupled to the inside of the vehicle through the windows, or apertures, resulting in a stochastic noise field inside. This noise field is then coupled onto circuitry inside the vehicle, designated as the RF Box in the figure. The circuitry on the box operates at much higher frequency scale when compared to the EMI wave; however, its size is small when compared to the vehicle and the

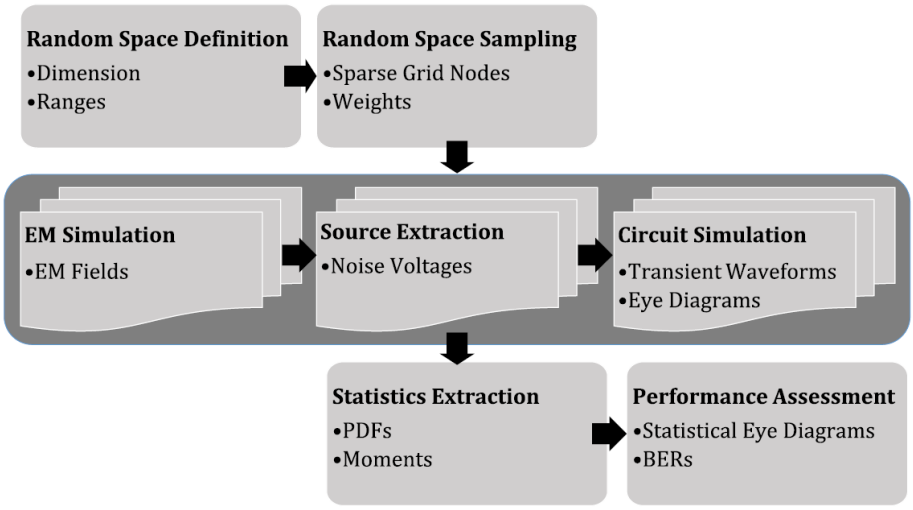

Figure 5.1: Workflow of multi-level and multi-scale EM/circuit stochastic simulation using SC.

wavelength of the EMI field. Nevertheless, the field coupled through the apertures manifests as noise voltages for the circuit on the board, and thus the output of the circuit is also stochastic. Furthermore, the geometry of the inside of the vehicle introduces additional reflections of the incident EMI field; thus, the solution of this problem contains many intermediate variables and is very expensive to obtain even in the deterministic case.

We analyze the problem by simulating the macroscopic problem in a commercial EM field solver, which outputs the EM field everywhere in the problem domain. Leveraging the fact that RF Box is electrically small compared to the scale of the EMI, we translate the calculated field on the surface of the RF Box into an equivalent noise voltage source. Then, we perform a circuit simulation of the circuitry inside the RF Box, superpositioning the noise voltage into the circuit, which allows us to obtain the results.

Leveraging black-box modeling and non-intrusive SC, we treat the entire problem as a single function. That is to say, the multi-level simulation takes EMI fields, including its randomness, as inputs, and obtains some circuit performance metric as outputs. In our case, we operate a high-speed signaling link on the circuit, and

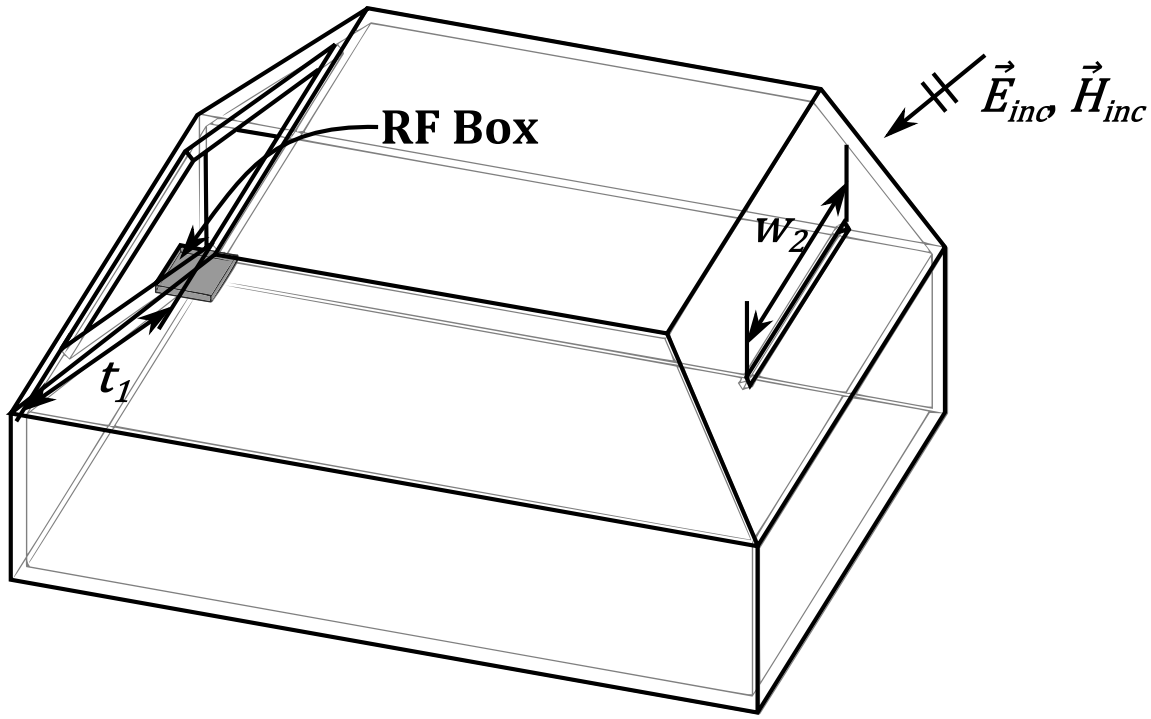

Figure 5.2: Vehicle with RF box situated inside at a fixed location. The height of the front aperture $t_1 \sim \mathcal{U}(0.2,\, 0.6)\,(\mathrm{m})$ and the width of the rear aperture $w_2 \sim \mathcal{U}(0.2,\, 1.0)\,(\mathrm{m})$ are random variables.

wish to study the effect of system-level EMI on the eye diagram opening of the link. Intermediate results include the stochastic noise voltage sources that we use in the circuit simulation, which must also be characterized. Numerical details and solutions are shown in Section 5.4.

5.3 Monte Carlo Evaluation of Interpolation Residual

The accuracy of SC is dependent on construction of an accurate interpolation of the outputs. For multi-level systems, the outputs are often high-order and non-smooth in the random domain. Thus it is necessary to calculate the error residual of the interpolation in order to evaluate the quality of interpolation. To decrease the residual, more nodes need to be added during construction. Globally, this can be done by increasing the level of interpolation, similar to $h-$refinement of the mesh, until a desired residual is achieved [21, 28, 48, 49]. Another approach is to locally increase the number of nodes in regions where the outputs are non-smooth, such as near resonance points, so that the additional nodes are optimally placed to capture the sharp variations in outputs. Both approaches require a method to calculate the residual of a given interpolation. This is often done by adding additional nodes via $h-$refinement, then comparing the interpolated outputs at these nodes with the actual calculated values. The disadvantage of this approach is that the nodes corresponding to a higher level of interpolation must be evaluated, which can be expensive, especially when dimensionality is high. A different approach, proposed in Section 5.3, is to estimate the residual by performing a small set of MC samples in the random space, then compare the values at these points with the interpolated values at various levels. This approach will eliminate the need to perform any additional deterministic simulations.

5.3.1 Residual Calculation

For a given interpolation $\tilde{f}_k(\vec{x})$ of level k, the residual can be calculated as:

$$r_k = \left\| \tilde{f}_k(\vec{x}) - f(\vec{x}) \right\|_2 = \int_D \left| \tilde{f}_k(\vec{x}) - f(\vec{x}) \right|^2 d\vec{x} \tag{5.3}$$

The integral is evaluated using quadrature rule defined over sparse grid of level $k+1$. The cost of evaluating the residual at each level is an additional $M_{d,k+1} - M_{d,k}$ number of runs, which grows unfavorably w.r.t. k and d. Here we choose to calculate the L_2 norm in (5.3), although other norms such as L_∞ would also suffice. The norm can be defined over the entire random domain D in case of global mesh refinement, or can be defined over a subdomain $\bar{D} \subset D$ to evaluate locally adaptive refinement.

For adaptive refinement, an iterative scheme is used where k is continually increased until a certain criterion $r_k < \epsilon$ is met. The threshold ϵ is defined by the user and is usually determined ad hoc. Although the residual is calculated exactly, the process for picking ϵ exactly is less clearly defined. Hence, we propose that there is little need to calculate r_k exactly, and an estimation via MC integration can be used instead:

$$\tilde{r}_k = V \frac{1}{N} \sum_{i=1}^{N} \left| \tilde{f}_k(\vec{x}_i) - f(\vec{x}_i) \right|^2 \tag{5.4}$$

$$V = \int_D 1 \, d\vec{x} \tag{5.5}$$

where $\Theta_{MC} = \{\vec{x}_i\}_{i=1}^N$ is a set of N MC input points generated based on uniform distribution over the random domain. The advantage of this estimation is that $\{f(\vec{x}_i)\}_{i=1}^N$ only needs to be calculated once, and the evaluation of $\{f_k(\vec{x}_i)\}_{i=1}^N$ is fast since it is interpolated. Furthermore, the convergence of MC is independent of the dimensionality of random space, making this method especially suitable for problems of high d. In fact, the error is proportional to $V\frac{\sigma_N}{\sqrt{N}}$, where σ_N is the sampled standard deviation of $f(\cdot)$ over the domain. This means that the method is less accurate for functions that are highly variant in the random space. On the other hand, the error of the sparse grid is proportional to $M^{-k}(\log M)^{(k+2)(d-1)+1}$, which

grows unfavorably w.r.t. d.

5.4 Numerical Example: RF Box in Vehicle

5.4.1 Full-wave Electromagnetic Simulation and Equivalent Noise Voltage Source Calculation

We consider the problem of evaluating the electromagnetic interference (EMI) from a $\theta-$polarized plane wave with $f = 320\,\text{MHz}$ incident upon a vehicle with apertures. The wave couples into the cavity of the vehicle via the apertures, and causes EMI on a RF box containing circuits placed in a fixed location within the vehicle. The vehicle is modeled using a PEC box with dimensions $2 \times 1.5 \times 1\,(\text{m}^3)$, hovering $0.2\,\text{m}$ above an infinite ground plane. The incident wave $(\vec{E}_{inc}, \vec{H}_{inc})$ approaches the vehicle at an angle of $(\phi, \theta) = (120^\circ, 70^\circ)$, with electric field magnitude $1\,\frac{\text{V}}{\text{m}}$. The sizes of the apertures constitute the random inputs of the problem, as illustrated in Figure 5.2. The EM problem is solved using a full-wave finite element boundary integral (FEBI) solver [50].

The fields on the RF box are used to calculate equivalent noise voltage sources on a transmission line. A circuit source solver is developed to provide the EMI noise sources. To obtain the EMI noise sources at ends of wire, we develop a comprehensive EM formulation. The solution procedure can be summarized as follows:

1. Coupling of external fields to modal fields in RF box.
2. Conversion of modal fields to the "impressed" fields of the microstrip lines.
3. Calculation of open-ended voltages on ends of wires.

The voltages at the nodes on ends of the microstrip represent the desired EMI noise sources, the magnitude of which will serve as an output function of interest $f(\vec{x})$ for this example.

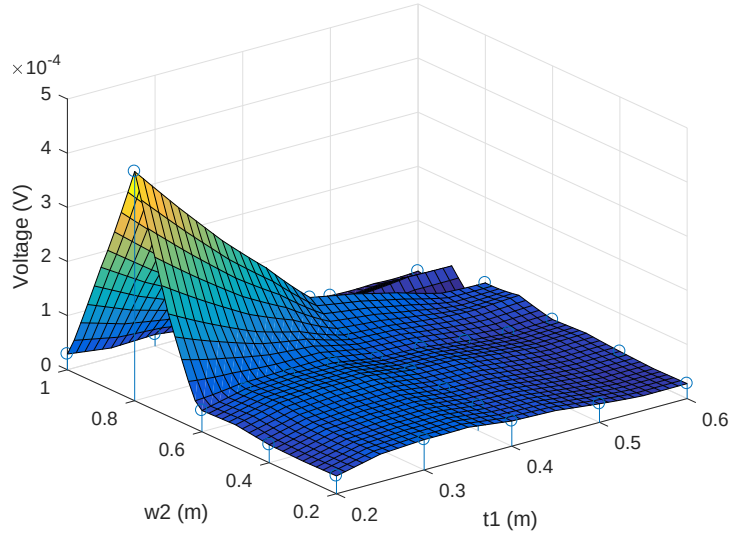

(a)

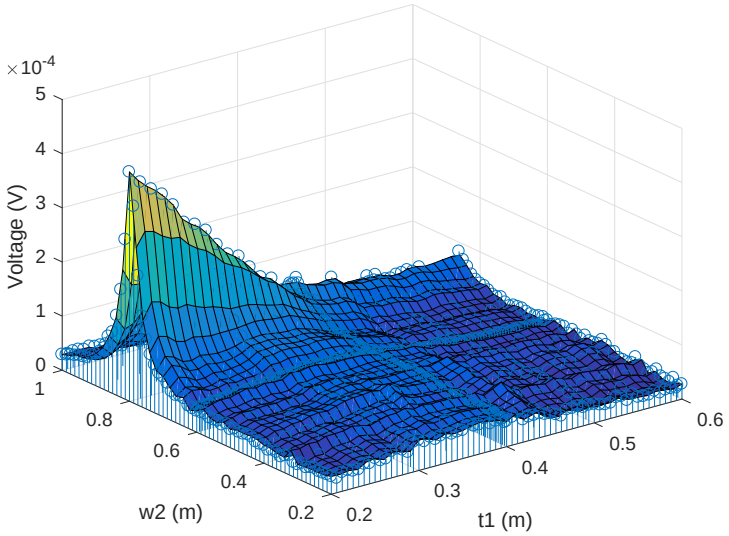

(b)

Figure 5.3: Interpolation $\tilde{f}(\vec{x}) = |V_{noise1}|$ for (a) $k = 3$ and (b) $k = 7$. The points shown are interpolation nodes.

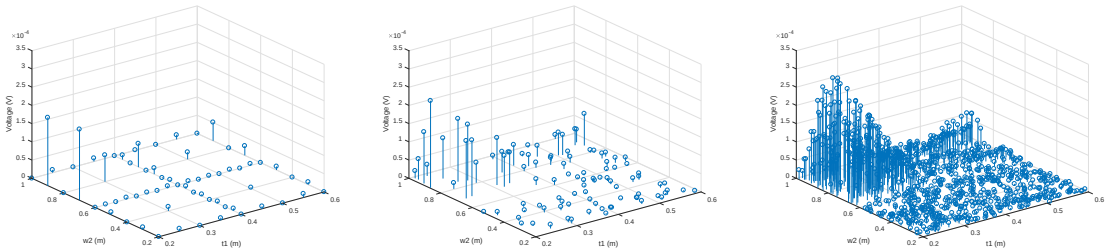

(a) $\left|\tilde{f}_3 - f\right|$ on $\Theta_{2,4}$ (b) $\left|\tilde{f}_3 - f\right|$ on $\Theta_{MC},\ N = 100$ (c) $\left|\tilde{f}_3 - f\right|$ on $\Theta_{MC},\ N = 1000$

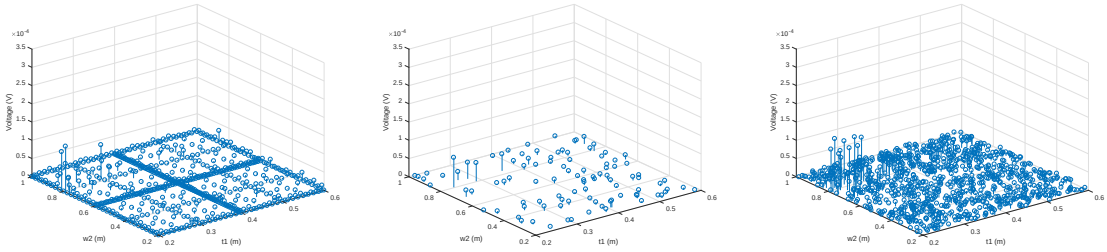

(d) $\left|\tilde{f}_6 - f\right|$ on $\Theta_{2,7}$ (e) $\left|\tilde{f}_6 - f\right|$ on $\Theta_{MC},\ N = 100$ (f) $\left|\tilde{f}_6 - f\right|$ on $\Theta_{MC},\ N = 1000$

Figure 5.4: Residual calculated at sparse grid nodes and Monte Carlo points for $k = 3$ and $k = 6$.

5.4.2 Interpolation Residuals

The simulation of the problems requires using a commercial EM solver, as well as a proprietary EMI noise extraction method outlined in Section 5.4.1. The entire process is encapsulated in a black-box. As can be seen, the system is complicated and we expect the solution to be high-order. We choose the magnitude of the equivalent complex voltage noise source as the output of interest. The response surface for $\tilde{f}(\vec{x}) = |V_{noise1}|$ is shown in Figure 5.3 for $k = \{3, 7\}$.

As can be seen, the function is non-smooth in the quadrant $0.2 \leq t_1 \leq 0.4,\ 0.6 \leq w_2 \leq 1.0$. The residuals calculated using (5.3) and (5.4) are shown in Figure 5.4 for $k = \{3, 6\}$. The convergence of L_2 norm of residual is shown in Figure 5.5.

As we can see from Figure 5.5, the estimation of residual $\tilde{r}_k$ converges asymptotically, similar to r_k. It is also interesting to note that $\tilde{r}_k$ for the $N = 100$ and

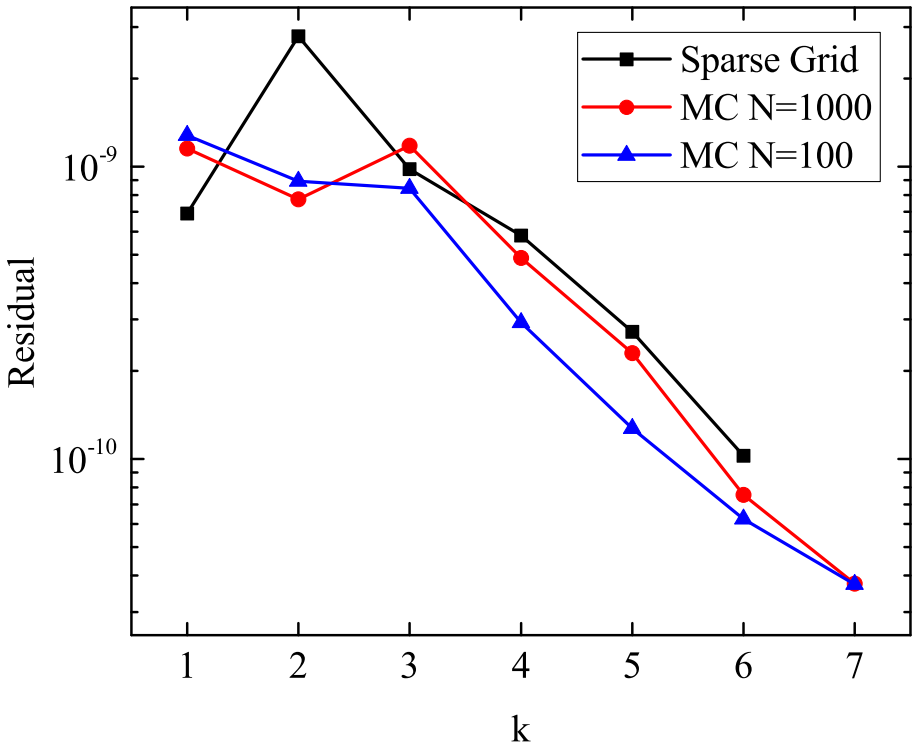

Figure 5.5: Convergence of L_2 norm of residual over the random space.

$N = 1000$ cases are quite close. This suggests that a small set of MC is enough to evaluate the quality of interpolation. An ad hoc convergence criterion ϵ needs to be defined for $\tilde{r}_k$ based on experience and engineering judgment. In Figure 5.5, $\tilde{r}_k$ is provided for $k = 7$ since the available data is sufficient to calculate this value. In order to calculate r_7, 832 additional deterministic simulations need to be performed. This demonstrates the advantage of the proposed method in that it allows the residual to be evaluated without further grid refinement. In addition, if $N = 100$ is used to estimate $\tilde{r}_k$, then we can see from Table 5.1 that the proposed technique becomes computationally advantageous at $k = 5$ for $d = 2$ and at $k = 2$ for $d = 6$. The method should also be applicable to $p-$refinement of the basis functions, and will be investigated in the future.

5.4.3 Stochastic Eye Diagram Characterization of Circuit in RF Box

To evaluate the effect of external RF interference on digital circuitry inside the vehicle, we perform eye diagram simulation of a high-speed signaling link on printed circuit board, situated inside the RF box.

The channel is constituted of a 10cm segment of microstrip transmission line. The excitation is a digital signal operating at 5 Gbps with bit time of 200 ps. The rise and fall times are both 50 ps. The source has 50Ω impedance and is connected in parallel with a 1 pF capacitor that models the pin capacitance. The receiver is modeled as a 50Ω load in parallel with a 1 pF capacitance also. The signal voltage is probed at the input of the load, as shown in Figure 5.6.

The noise from external EM field is modeled as two AC voltage noise sources, connected in series on both sides of the transmission line. The magnitude and phase of the voltage are stochastic and vary with the random variables in the system. The randomness in this example results from the size of the aperture on the vehicle, which is modeled during the EM modeling phase.

The transient simulation is performed for 500 ns, which represents approximately 2500 digital bits of data. The data stream is pseudo-random bit sequence (PRBS). By overlapping the voltage plot of each bit at the output, we can construct an eye

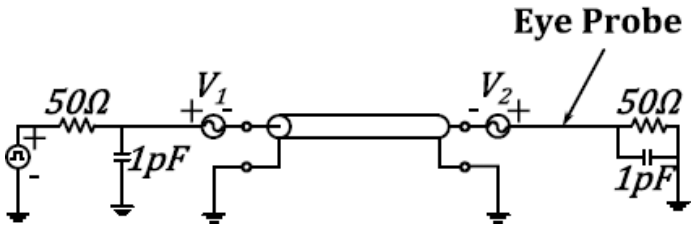

Figure 5.6: Circuit for simulating eye diagram of 5 Gbps signal with RF interference.

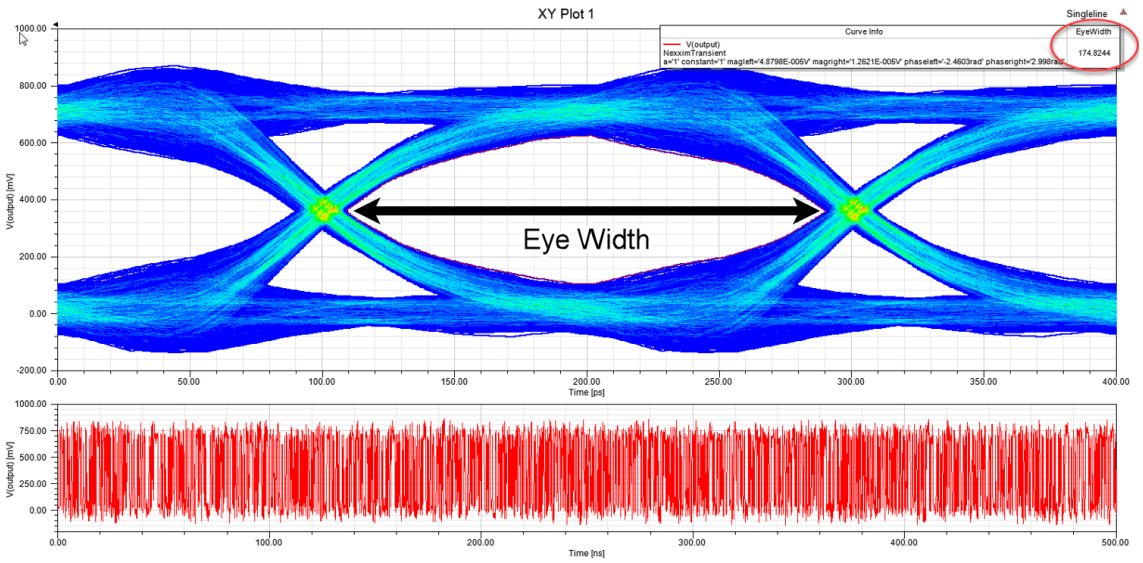

Figure 5.7: Eye diagram of the voltage seen at receiver input. The measured eye width is shown at upper right corner of the plot.

diagram, which is shown in Figure 5.7.

The eye width is used as the cost function to measure the performance of the signaling link with noise. Thus, a response surface of the eye width in random space is constructed using Smolyak sparse grid with $d = 2$ dimension and $k = 7$ interpolation levels. A total of 705 deterministic simulations is needed to construct this response surface. As can be seen in Figure 5.8, the response surface shows that the eye width experiences a sharp drop in random space near where the width of aperture 2 is about a wavelength wide. This same phenomenon can be seen in the

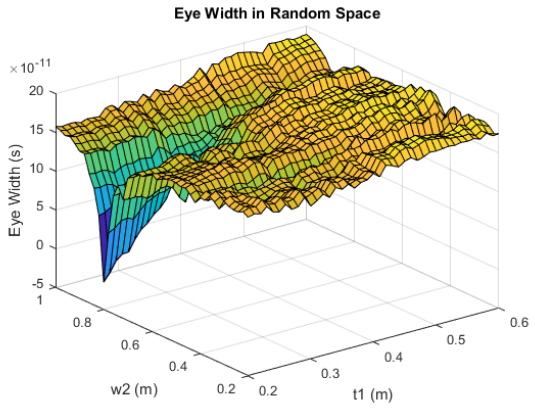

Figure 5.8: Response surface of eye width in random space.

response surface of the noise voltage magnitude in Figure 5.9, where it can be seen that the noise voltage increases at the same location in random space. What we observe here makes sense as a higher noise magnitude corresponds to a smaller eye opening, and thus lower performance of the signaling link.

As can be seen from this example, there is non-smooth behavior of the response surface for our cost function in localized regions of the random space. This highlights the need for further research in adaptive sparse grid refinement, which will allow us to add collocation nodes near the highly sensitive regions without needing to refine the grid over the entire random space.

The probability density function (PDF) of the eye width can be generated by performing Monte Carlo integration over the response surface. A comparison of the Stochastic Collocation results and Monte Carlo results is shown in Figure 5.10. Failure of the signaling link will correspond to cases where the eye width is smaller than a threshold, thus the accuracy of the left-most tail of the PDF is the most important aspect of our stochastic modeling. As the results show, we model the tail quite accurately.

We also observe that in regions of the random space where noise signal is strongest, a clear closing of the eye opening can be seen as a localized and sharp drop in eye width. This is consistent with what is expected.

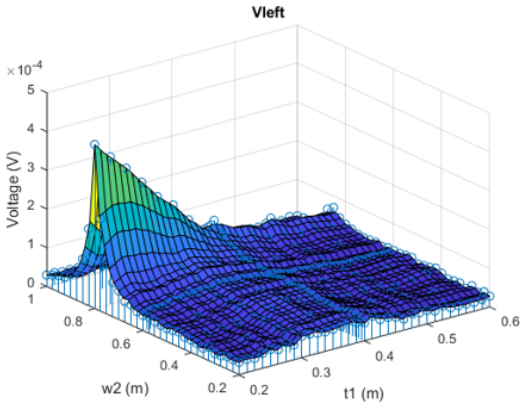

(a) V_1 (left)

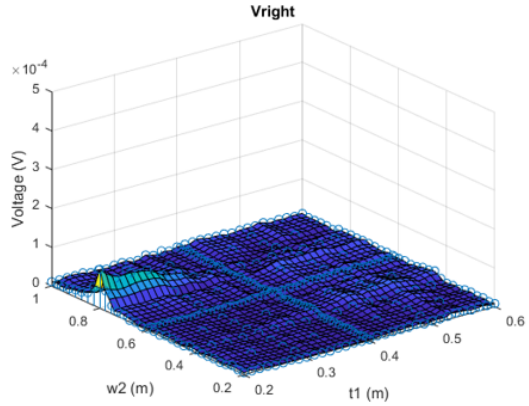

(b) V_2 (right)

Figure 5.9: Response surface of noise voltage source 1 and noise voltage source 2.

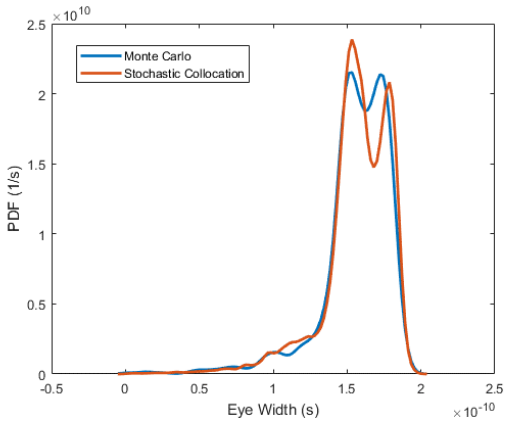

Figure 5.10: PDF of eye width calculated using SC and MC.

5.5 Adaptive Stochastic Collocation Using Wavelet Basis

In the previous section, the problem under consideration shows sharp localized behavior in the cost functions. Rather than using uniform interpolation rules to capture this locally sharp behavior, adaptive schemes can be used to add interpolation nodes where the function is least smooth. In general, the behavior of practical electromagnetic and circuit systems often depends strongly on variations in physical parameters. Uncertainties in internal components due to manufacturing imperfections such as device and interconnect sizes create a need for the statistical characterization of system outputs. Non-intrusive stochastic numerical techniques sample solutions from deterministic simulation software to calculate desired statistical information. These are the methods of choice in most engineering problems; re-implementation of existing deterministic simulation software to produce solutions using random variable expansions, i.e. using intrusive methods, is often impractical and computationally expensive.

Non-intrusive sampling methods compute deterministic solutions for a set of input points in the random parameter space. Monte Carlo (MC) sampling methods are the most commonly used and straightforward methods for computing statistical moments. A large set of deterministic solutions is computed using inputs sampled from the PDFs of random parameters. While MC scales well with number of random

parameters, convergence is slow as great many deterministic solutions are required.

Alternatively, a behavioral interpolation model of the system response in the random space can be created, e.g. using a global polynomial expansion. These methods use a "sparse grid" of sampling points that allows for faster-than-MC convergence, assuming the system behaves smoothly in the random space. Many common electrical systems exhibit irregularities and steep gradients and require adaptive techniques such as multi-element methods [21], multi-resolution approximations [51], and hierarchcial sparse grids [52, 24]. These methods dynamically increase sampling density in irregular regions.

Scaling these methods to high-dimensional problems with many random parameters is difficult; tensor product decompositions lead to dense systems, and sampling grid sizes cannot be truly minimized without rigorous refinement criteria. The adaptive wavelet stochastic collocation method (AWSCM) proposed in [53] attempts to overcome these problems using a sparse hierarchical grid structure and wavelet basis functions whose expansion coefficients can be used as rigorous refinement criteria. Because of this, wavelet approximations potentially require minimal deterministic solutions to meet error criteria.

5.5.1 Hierarchical Sparse Grids and Adaptive Refinement

The method in this chapter uses the hierarchical sparse grids described in [24] as a sparse sampling strategy. Denoting points in the N-parameter random space as $\boldsymbol{x} \in \mathbb{R}^N$, an M-point approximation $\tilde{f}(\boldsymbol{x})$ for the system response $f(\boldsymbol{x})$ can be constructed as:

$$\tilde{f}(\boldsymbol{x}) = \sum_{j=1}^{M} w_j \psi_j(\boldsymbol{x}_j) \tag{5.6}$$

This is a linear combination of basis functions ψ_j evaluated at the grid points $\boldsymbol{x}_j$. Points are grouped into integer scaling levels in a recursive hierarchical structure. Except for the uppermost points on level 0, each point in this structure stems from

parent points on the level above. An adaptive refinement strategy can be devised to select parent points to spawn nearby child nodes; points on deeper levels are more closely spaced and are able to resolve more detailed features.

A level l approximation $\tilde{f}_l$ can be refined to $l+1$ using K new grid points $\boldsymbol{x}_k$ and (5.7); associated weights w_k are computed from associated deterministic solutions $f(\boldsymbol{x}_k)$ so that the linear system in (5.6) is satisfied.

$$\tilde{f}_{l+1}(\boldsymbol{x}) = \tilde{f}_l(\boldsymbol{x}) + \sum_{k=1}^{K} w_k \psi_k(\boldsymbol{x}_k) \tag{5.7}$$

5.5.2 Second-Generation Wavelets

Second-generation biorthogonal wavelets are an effective choice for the basis functions ψ_j as they allow for a multiresolution approximation that fits the hierarchical, nonuniform grid structure necessary for adaptive sampling. In an update step, new weights w_k can be directly computed as:

$$w_k = f_{l+1}(\boldsymbol{x}_k) - \tilde{f}_l(\boldsymbol{x}_k) \tag{5.8}$$

Additionally, since wavelets form a Riesz basis, coefficient magnitudes $|w_j|$ strongly indicate the contributions of their associated basis terms to the interpolation; large magnitudes indicate the presence of local features and a need for refinement. Standard finite element bases, such as linear hierarchical piecewise polynomials, are not Riesz bases, and are shown to require potentially more grid points to achieve the same level of accuracy when using a coefficient-driven adaptive refinement strategy in [53]. Other Riesz bases, such as Fourier complex exponentials, tend to be globally supported and unsuitable for characterizing local behavior.

First-generation orthogonal wavelets form a multiresolution approximation local in both the frequency and spatial domains by means of scaled and shifted compact wavelet basis functions. Second-generation wavelets generalize this concept to arbitrary domains with irregularly spaced data, such as in the sparse grid framework.

The lifting scheme is used to derive basis functions in the random parameter domain on different resolution levels. Interpolating wavelets are used for the numerical example, and are lifted out of the piecewise linear hierarchical basis through subdivision following the procedures in [53, 54].

5.5.3 Adaptive Refinement Strategy

Generally, a priori knowledge of system behavior is necessary to tailor an optimal sampling strategy. However, a quasi-optimal sampling scheme can often be devised using coefficient magnitudes $|w_j|$ and the refinable grid structure described. The strategy in the numerical example is based on the family direction selective strategy described in [52, 24, 55]. Accounting for natural grid structure and stability considerations, only the points surrounding those with high $|w_j|$ are selected for refinement.

An initial grid should be chosen to be as sparse as possible, yet dense enough to trigger refinement near important dynamics to ensure approximation convergence. Additionally, the choice of coefficient threshold affects convergence rate as well as stability. This threshold is chosen ad hoc but is dynamically increased to limit the refinement points added in any single refinement step, with the goal of enforcing stability and improving convergence rate. As illustrated in Figure 5.11, refinement continues until an approximate maximum allowable grid size is reached, depending on available computational resources.

5.6 Numerical Example: RLC Resonator Circuit

The adaptive wavelet refinement scheme is tested using a resonant RLC circuit example from [21]. The circuit shown in Figure 5.12 is selected for its sharp voltage characteristics. It consists of a lossless transmission line (TL) terminated by an RLC circuit and is excited by a sinusoidal voltage source at $f = 486.28$ MHz. The real and imaginary components of the voltage across the capacitor, $Re\{V_c\}$ and $Im\{V_c\}$, are chosen as observable outputs. As shown in Figure 5.13, V_c varies rapidly as pa-

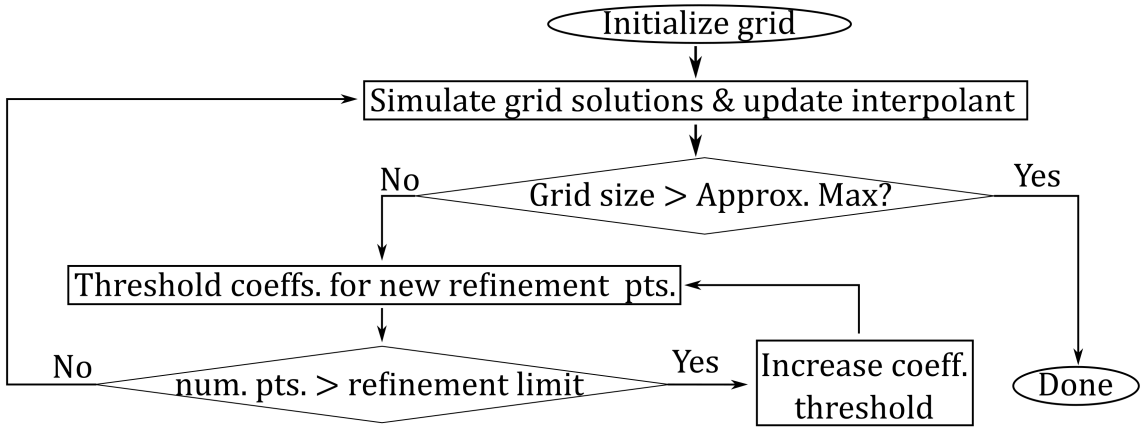

Figure 5.11: Flowchart of the Adaptive Wavelet Stochastic Collocation Method, with feedback adaptive refinement.

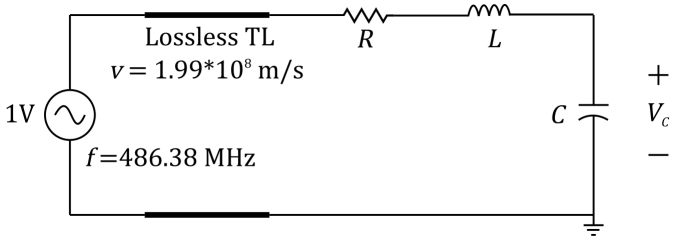

Figure 5.12: Lossless transmission line terminated by an RLC circuit, showing parameters used in 2D interpolation.

rameters approach resonant values. The TL has wave speed $v = 1.99 \times 10^8$ m/s, characteristic impedance Z_0, and length l. It is terminated by a resistor with value $R = 2\Omega$ in series with an inductor and capacitor, parameterized by L and C. Using $\Gamma_L = \frac{R+j\omega L+\frac{1}{j\omega C}-Z_0}{R+j\omega L+\frac{1}{j\omega C}+Z_0}$, the analytical phasor solution for V_c is given by:

$$V_c = \left(\frac{(1+\Gamma_L)}{e^{j\frac{2\pi f}{v}l} + \Gamma_L e^{-j\frac{2\pi f}{v}l}}\right)\left(\frac{\frac{1}{j\omega C}}{R + j\omega L + \frac{1}{j\omega C}}\right) \tag{5.9}$$

We will look at two scenarios. In the first case Z_0 and l are fixed, and L and C are random. Then we will look at the second case where all four variables are random. In both cases, there is sharp resonance in the response surface of V_c in the random space.

5.6.1 Interpolation with Two Random Parameters

TL characteristic impedance and length are first fixed at $Z_0 = 50\Omega$ and $l = 0.4$ m, and L and C are uniformly distributed between $[5, 15]$ nH and $[10, 20]$ pF. Figure 5.13 visually shows the wavelet approximation of V_c as well as the grid used to approximate $Re\{V_c\}$, which demonstrates adaptive refinement in non-smooth regions.

5.6.2 Interpolation with Four Random Parameters

Approximation convergence rate is evaluated for the parameters in Section 5.5.1 as well as the case when l and Z_0 are also uniformly distributed between $[0.3, 0.5]$ m and $[40, 60]$ Ω. Average residual is used as an error metric and can be estimated on a parameter space D with volume V_D using a quadrature rule:

$$\bar{\rho} = \frac{1}{V_D}\int_D \left|f(\boldsymbol{x}) - \tilde{f}(\boldsymbol{x})\right|^2 d\boldsymbol{x} \tag{5.10}$$

Approximations using linear piecewise polynomials with the same hierarchical gridding and refinement strategy and a non-adaptive classical sparse grid with a global Clenshaw-Curtis interpolation rule are used for comparison. Figure 5.14 shows aver-

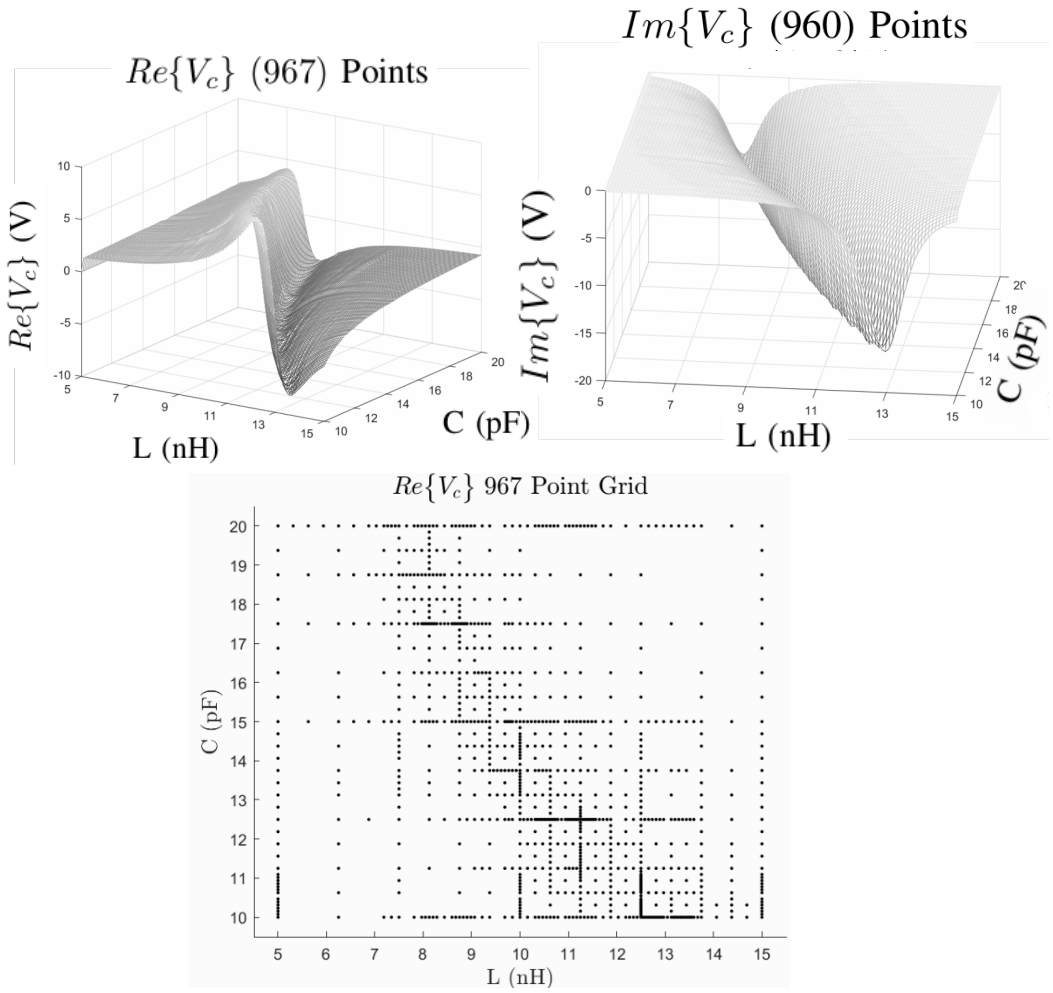

Figure 5.13: Approximated $Re\{V_c\}$ and $Im\{V_c\}$ using approx. 1000 points and adaptive grid used to approximate $Re\{V_c\}$ with 967 points.

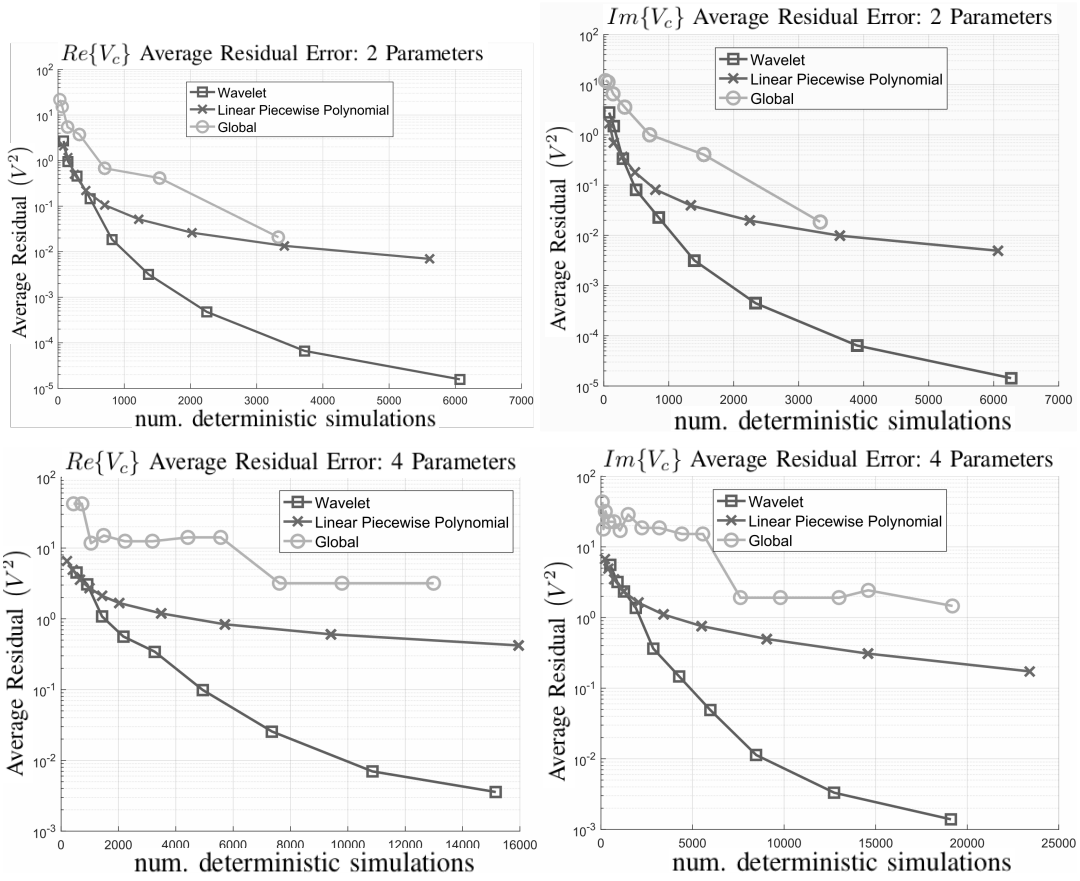

Figure 5.14: Residual (log scale) vs. grid size for wavelet, linear piecewise polynomials, and non-adaptive global grids for two and four random parameters.

age residuals for increasing grid size. The adaptive grids are initialized with around 200 points, and $\bar{\rho}$ is plotted at each refinement step. The global grid is not refined, but created with increasing grid densities. AWSCM shows superior convergence rate and dimension scaling, outperforming the other two methods. The global grid is competitive for two parameters but struggles with four, demonstrating the need for adaptive sampling in high-dimensional problems.

5.7 Conclusions

In this chapter, a non-intrusive SC approach is demonstrated to be effective at solving stochastic problems of multi-level and multi-scale systems. This system-level approach to stochastic modeling and simulation allows existing tools, both commercial and proprietary, to be used in the uncertainty quantification process. There are challenges to using an SC approach for solving problems exhibiting resonant behavior in the random domain, and a method was proposed to address this challenge. The results suggest that using adaptive wavelet basis to perform SC can alleviate some of the computational inefficiencies with constructing a resonant response surface. Overall, non-intrusive techniques such as SC are very powerful since they enable the solution of stochastic problems for all classes of problems where deterministic solvers already exist. In practice, this utility allows complex systems to be solved without the need to reformulate the system equations. Hence, such an approach can have broad appeal to industry and EDA tool developers.

CHAPTER 6

DISCUSSION AND FUTURE RESEARCH

6.1 Discussion

To simulate large and high-order systems with uncertainties, it is important to choose the appropriate numerical approach for each situation. Numerically complex tasks such as full-wave electromagnetic simulations and parameter extractions are best performed using a sampling technique. Accelerated sampling techniques such as SC are appropriate when the dimensionality of random space is manageable. Techniques such as adaptive refinement can help achieve desired simulation accuracy without sacrificing computation time.

On the other hand, numerically simpler tasks such as circuit and transmission line simulation with LIM are implemented most efficiently using non-sampling techniques, due to their accuracy. The curse of dimensionality still exists in this case, and the same benefits from dimensionality reduction still apply..

Overall, however, it is important that different techniques can be used for separate parts of the overall simulation. Currently, simulations for signal and power integrity involve using multiple tools in several steps to obtain the measure of interest. The EM extraction can be done using SC, and the relevant equivalent circuit parameters can be extracted. In this case, the extracted parameters will be expansion coefficients for gPC expansion of the circuit parameters. Then, a fast stochastic simulator such as Stochastic LIM can be used to obtain the time-domain results quickly and efficiency.

These techniques combined allow us to study multi-level and resonant problems where uncertainties permeate the system. The simulation of these systems are expen-

sive even when performed deterministically, making traditional statistical simulations intractable. Fast techniques such as those presented in this document allow the effect of uncertainties to be quantified in these cases.

6.2 Future Research

The results presented in this thesis represent significant progress in applying stochastic numerical and uncertainty quantification techniques to study EM and circuit problems. Nevertheless, they also suggest several future research directions that can bring further advancements to the state of the art.

6.2.1 Stochastic High-Speed Link Simulator

Although transient simulations are traditionally used to evaluate performance of electrical interconnects, many modern high-speed serial links are evaluated using information metrics such as bit error rate (BER). In such serial links, the typical BER is on the order of 10^{-13}. In other words, a large number of bits must be simulated before a data error occurs. Given the corresponding length of transient simulation needed to simulate this amount of data, approaches like Stochastic LIM simply cannot solve problems of this scale. Rather, statistical methods are typically used to construct the so-called statistical eye diagrams, which estimate the BER by convolution of the bit response of the link with probability mass functions of the data. Current methods account for deterministic jitter that results from channel degradation, as well as random jitter which comes from process and thermal uncertainties in the driver and receivers. However, a stochastic model of the channel is not included in currently available tools. A high-speed link simulator compatible with stochastic channel models will be very useful for evaluating the performance of links in extreme environments. For instance, in aerospace applications, the printed circuit board containing the channel for high-speed USB links experiences rapid and significant changes in the amount of moisture absorbed by the substrate. The dielectric

property of the board will vary due to the moisture content, and thus the electrical model of the channel is inherently stochastic. An efficient method can be developed to expediently evaluate situations such as this.

6.2.2 Stochastic Macromodels

Instead of equivalent lumped circuit models, many interconnect components are modeled using transfer functions. This is desirable because the models for more complicated structures such as vias and connectors exhibit strong frequency-dependent behavior. In fact, transmission lines such as those studied in this thesis are often modeled as network parameters in order to account for the dispersive property of dielectric substrate and frequency-dependent loss effects such as skin effect and proximity effect. The limitation of such models is that they are very specific to the structure being modeled. For instance, a set of network parameters needs to be generated for a specific length of transmission line, and separate models need to be generated for via model with different center-to-center spacing. The generation of these models utilizes 3D EM field solvers and is rather expensive. It is desirable to create compact and parameterized transfer functions that can represent the behavior of such interconnects. With parameterized macromodels, analysis of uncertainty in such structures can be performed using sampling techniques, without the need to generate full 3D models for each instantiation. Methods need to be developed to parameterize transfer functions, to reduce the order and size of these macromodels, and to construct the relationship between input parameters and model parameters in an automated fashion, so that even complicated structures exhibiting uncertainties can be simulated. Furthermore, methods need to be developed to incorporate the stochastic macromodels in tools like Stochastic LIM and the stochastic high-speed link simulator proposed above, so these models can be used to obtain the desirable outputs.

6.2.3 Stochastic FDTD for Transient EM Field Analysis

The Stochastic LIM presented in this thesis is an improvement over regular LIM, which is a circuit simulator that uses many of the same numerical techniques as the popular finite-difference time-domain (FDTD) technique for EM field solution. Hence it should be possible to follow steps similar to those demonstrated in this thesis to construct an intrusive formulation of the FDTD field update equations, thus making a transient EM field solver capable of solving fields when the properties of materials and medium are uncertain. This will be very useful for simulating microwave dosimetry problems, since human tissue varies by each individual, and a stochastic simulation can provide information that leads to designs which are robustly safe but not overly conservative and which do not sacrifice functionality for lower cost.

6.2.4 Sequential Function Approximation for Big Data Analysis

The SC method as presented in this thesis utilizes pre-defined nodes where the function must be evaluated in order to construct an interpolation. In practice, it would be desirable to construct an interpolation or an approximation of the cost function using previously available data. This is the big data approach to modeling distinct classes of problems. For example, microstrips are ubiquitous in industry and many models have been constructed for these structures. It would be good to take collections of past models and their corresponding inputs, and use them to construct an approximation of the model in terms of one or several parameters. For SC, data must be provided for specific nodes in the parameter space. But recently developed techniques have shown that sequential functional approximation can construct approximations using past data, even if they are clustered in the input parameter space. Although as an interpolation, these techniques are not as efficient as sparse grid for SC, they do have utility since all previously available data can be used to improve the quality of the interpolated model. For modeling structures that are commonly used across the industry and for which many models and outputs exist, the big data approach can achieve the objects of sparse grid without needing to run any addi-

tional simulations at all. In addition, sequential function approximation has been shown to be efficient for problems with high-dimensional input ($d > 100$). It will be interesting to apply these techniques to problems in the EM and circuit simulation area.

6.2.5 Experimental Verification of Stochastic Simulation Results

The vast majority of the results presented in this thesis are verified using prior techniques such as MC. Although the results correlate well, no correlation with lab hardware measurement is performed. There are many unique challenges that must be overcome in order to perform uncertainty quantification measurements in hardware. The foremost concern is cost, since a large sample size of hardware must be fabricated and each one must be characterized. The proper identification of input parameter values and consistency of output measurements are also challenging, since the measured output will unavoidably contain noise. Finally, much thought can be given to applying fast uncertainty quantification methods used in simulations for this thesis to measurements, so the statistics can be measured with many fewer samples. Experimental results can also be used with sequential function approximation to calibrate and refine stochastic models.

REFERENCES

[1] D. V. Ginste, D. D. Zutter, D. Deschrijver, T. Dhaene, P. Manfredi, and F. Canavero, "Stochastic modeling-based variability analysis of on-chip interconnects," *Packaging and Manufacturing Technology IEEE Transactions on Components*, vol. 2, no. 7, pp. 1182–1192, July 2012.

[2] P. Manfredi and F. G. Canavero, "Statistical prediction of temperature effects inside through-silicon vias by means of orthogonal polynomials," in *Microwave Symposium Digest (MTT), 2012 IEEE MTT-S International*. IEEE, 2012, pp. 1–3.

[3] P. Manfredi, D. V. Ginste, D. D. Zutter, and F. G. Canavero, "Generalized decoupled polynomial chaos for nonlinear circuits with many random parameters," *IEEE Microwave and Wireless Components Letters*, vol. 25, no. 8, pp. 505–507, Aug. 2015.

[4] J. Ochoa and A. Cangellaris, "Random-space dimensionality reduction scheme for expedient analysis of microwave structures with manufacturing variability," in *Proc. IEEE MTT-S Int. Microwave Symp. Digest (MTT)*, June 2013, pp. 1–3.

[5] J. S. Ochoa and A. C. Cangellaris, "Random-space dimensionality reduction for expedient yield estimation of passive microwave structures," *IEEE Transactions on Microwave Theory and Techniques*, vol. 61, no. 12, pp. 4313–4321, Dec. 2013.

[6] J. S. Ochoa and A. C. Cangellaris, "Homogenization technique for transmission lines with random permittivity profiles," in *Proc. 17th IEEE Workshop Signal and Power Integrity*, May 2013, pp. 1–4.

[7] A. K. Prasad, M. Ahadi, and S. Roy, "Multidimensional uncertainty quantification of microwave /RF networks using linear regression and optimal design of experiments," *IEEE Transactions on Microwave Theory and Techniques*, vol. 64, no. 8, pp. 2433–2446, Aug. 2016.

[8] I. S. Stievano, P. Manfredi, and F. G. Canavero, "Parameters variability effects on multiconductor interconnects via hermite polynomial chaos," *Packaging and Manufacturing Technology IEEE Transactions on Components*, vol. 1, no. 8, pp. 1234–1239, Aug. 2011.

[9] T. Zhang, X. Chen, J. E. Schutt-Ainé, and A. C. Cangellaris, "Statistical analysis of fiber weave effect over differential microstrips on printed circuit boards," in *Proc. IEEE 18th Workshop Signal and Power Integrity (SPI)*, May 2014, pp. 1–4.

[10] X. Chen, J. E. Schutt-Ainé, and A. C. Cangellaris, "A strategy to optimize modal signaling over microstrip lines with spacing variability," in *Proc. 17th IEEE Workshop Signal and Power Integrity*, May 2013, pp. 1–4.

[11] X. Chen, J. S. Ochoa, J. E. Schutt-Ainé, and A. C. Cangellaris, "Optimal relaxation of I/O electrical requirements under packaging uncertainty by stochastic methods," in *Proc. IEEE 64th Electronic Components and Technology Conf. (ECTC)*, May 2014, pp. 717–722.

[12] N. Wiener, "The homogeneous chaos," *American Journal of Mathematics*, vol. 60, no. 4, pp. 897–936, 1938.

[13] R. G. Ghanem and P. D. Spanos, *Stochastic Finite Elements: A Spectral Approach*. New York: Springer-Verlag, 1991.

[14] D. Xiu and G. E. Karniadakis, "The Wiener–Askey polynomial chaos for stochastic differential equations," *SIAM Journal on Scientific Computing*, vol. 24, no. 2, pp. 619–644, 2002.

[15] D. Xiu, "Fast numerical methods for stochastic computations: A review," *Communications in Computational Physics*, vol. 5, no. 2-4, pp. 242–72, Feb. 2009.

[16] D. Xiu, *Numerical Methods For Stochastic Computations: A Spectral Method Approach*. Princeton, N.J.: Princeton University Press, 2010.

[17] K. Strunz and Q. Su, "Stochastic formulation of SPICE-type electronic circuit simulation with polynomial chaos," *ACM Transactions on Modeling and Computer Simulation*, vol. 18, no. 4, 2008.

[18] A. Biondi, D. V. Ginste, D. De Zutter, P. Manfredi, and F. G. Canavero, "Variability analysis of interconnects terminated by general nonlinear loads," *IEEE Transactions on Components, Packaging and Manufacturing Technology*, vol. 3, no. 7, pp. 1244–1251, 2013.

[19] Y. Cheng and L. J. Jiang, "Stochastic Galerkin methods for transient Maxwell's equations with random geometries," in *Antennas and Propagation (APSURSI), 2016 IEEE International Symposium on*. IEEE, 2016, pp. 2099–2100.

[20] D. Xiu and J. S. Hesthaven, "High-order collocation methods for differential equations with random inputs," *SIAM Journal on Scientific Computing*, vol. 27, no. 3, pp. 1118–1139, 2005.

[21] A. C. Yücel, H. Bağcı, and E. Michielssen, "An adaptive multi-element probabilistic collocation method for statistical EMC/EMI characterization," *IEEE Transactions on Electromagnetic Compatibility*, vol. 55, no. 6, pp. 1154–1168, Dec. 2013.

[22] A. C. Yücel, H. Bağcı, and E. Michielssen, "An ME-PC enhanced HDMR method for efficient statistical analysis of multiconductor transmission line networks," *Packaging and Manufacturing Technology IEEE Transactions on Components*, vol. 5, no. 5, pp. 685–696, May 2015.

[23] M. Ahadi and S. Roy, "Sparse linear regression (spliner) approach for efficient multidimensional uncertainty quantification of high-speed circuits," *IEEE Transactions on Computer-Aided Design of Integrated Circuits and Systems*, vol. 35, no. 10, pp. 1640–1652, Oct. 2016.

[24] M. Stoyanov, "Hierarchy-direction selective approach for locally adaptive sparse grids," Oak Ridge National Laboratory, One Bethel Valley Road, Oak Ridge, TN, Tech. Rep. ORNL/TM-2013/384, 2013.

[25] M. K. Stoyanov and C. G. Webster, "A dynamically adaptive sparse grids method for quasi-optimal interpolation of multidimensional functions," *Computers & Mathematics with Applications*, vol. 71, no. 11, pp. 2449–2465, 2016.

[26] A. Klimke and B. Wohlmuth, "Algorithm 847: spinterp: piecewise multilinear hierarchical sparse grid interpolation in MATLAB," *ACM Transactions on Mathematical Software*, vol. 31, no. 4, pp. 561–579, Dec. 2005.

[27] F. Nobile, R. Tempone, and C. G. Webster, "An anisotropic sparse grid stochastic collocation method for partial differential equations with random input data," *SIAM Journal on Numerical Analysis*, vol. 46, no. 5, pp. 2411–2442, 2008.

[28] N. Agarwal and N. R. Aluru, "A domain adaptive stochastic collocation approach for analysis of MEMS under uncertainties," *Journal of Computational Physics*, vol. 228, no. 20, pp. 7662–7688, 2009.

[29] A. Rong and A. C. Cangellaris, "Transient analysis of distributed electromagnetic systems exhibiting stochastic variability in material parameters," in *General Assembly and Scientific Symposium, 2011 URSI*, Aug. 2011, pp. 1–4.

[30] P. Manfredi, D. Vande Ginste, D. De Zutter, and F. Canavero, "Stochastic modeling of nonlinear circuits via SPICE-compatible spectral equivalents," *Circuits and Systems I: Regular Papers, IEEE Transactions on*, 2014, to be published.

[31] P. Balaban and J. Golembeski, "Statistical analysis for practical circuit design," *Circuits and Systems, IEEE Transactions on*, vol. 22, no. 2, pp. 100–108, Feb. 1975.

[32] T. E. Lovett, A. Monti, and F. Ponci, "Automatic synthesis of uncertain models for linear circuit simulation: A polynomial chaos theory approach," *Simulation Modelling Practice and Theory*, vol. 16, no. 7, pp. 796 – 816, 2008.

[33] J. E. Schutt-Aine, "Latency insertion method (LIM) for the fast transient simulation of large networks," *Circuits and Systems I: Fundamental Theory and Applications, IEEE Transactions on*, vol. 48, no. 1, pp. 81–89, Jan. 2001.

[34] J. Schutt-Aine, "Stability analysis for semi-implicit LIM algorithm," in *Microwave Conference, 2009. APMC 2009. Asia Pacific*, Dec. 2009, pp. 1270–1272.

[35] S. M. Smith, "Stochastic finite-difference time-domain," Ph.D. dissertation, Dept. Elect. and Comp. Eng., Univ. of Utah, Salt Lake City, UT, May 2011.

[36] R. Edwards, A. Marvin, and S. Porter, "Uncertainty analyses in the finite-difference time-domain method," *Electromagnetic Compatibility, IEEE Transactions on*, vol. 52, no. 1, pp. 155–163, Feb. 2010.

[37] Z. Deng and J. E. Schutt-Aine, "Stability analysis of latency insertion method (LIM)," in *Electrical Performance of Electronic Packaging - 2004*, Oct 2004, pp. 167–170.

[38] A. Klimke, "Sparse grid interpolation toolbox," Jan. 2006. [Online]. Available: http://www.ians.uni-stuttgart.de/spinterp/

[39] A. Klimke, *Sparse Grid Interpolation Toolbox - User's Guide*, Germany, Feb. 2008.

[40] M. Stoyanov, *User Manual: TASMANIAN Sparse Grids v3.1*, Oak Ridge National Laboratory, Feb. 2016. [Online]. Available: http://tasmanian.ornl.gov/manuals.html

[41] X. Chen, J. E. Schutt-Ainé, and A. C. Cangellaris, "Stochastic LIM for transient simulations of printed circuit board transmission lines with uncertainties," in *Proc. IEEE 66th Electronic Components and Technology Conf. (ECTC)*, May 2016, pp. 2297–2304.

[42] X. Chen, J. E. Schutt-Ainé, and A. C. Cangellaris, "Finite difference schemes for transient simulation of transmission lines exhibiting uncertainties," in *Proc. IEEE 20th Workshop Signal and Power Integrity (SPI)*, May 2016, pp. 1–3.

[43] S. N. Lalgudi, M. Swaminathan, and Y. Kretchmer, "On-chip power-grid simulation using latency insertion method," *IEEE Transactions on Circuits and Systems I: Regular Papers*, vol. 55, no. 3, pp. 914–931, April 2008.

[44] T. Sekine and H. Asai, "Block-latency insertion method (block-LIM) for fast transient simulation of tightly coupled transmission lines," *IEEE Transactions on Electromagnetic Compatibility*, vol. 53, no. 1, pp. 193–201, Feb. 2011.

[45] X. Chen, M. Qiu, J. E. Schutt-Ainé, and A. C. Cangellaris, "Stochastic LIM for transient simulation of circuits with uncertainties," in *Proc. IEEE 23rd Conf. Electrical Performance of Electronic Packaging and Systems*, Oct. 2014, pp. 29–32.

[46] D. Xiu, *Numerical Methods for Stochastic Computations: A Spectral Method Approach*. Princeton University Press, 2010.

[47] X. Ma, X. Chen, A. Rong, J. E. Schutt-Aine, and A. C. Cangellaris, "Stochastic electromagnetic-circuit simulation for system-level EMI analysis," in *Proc. IEEE Int. Symp. Electromagnetic Compatibility Signal/Power Integrity (EMCSI)*, Aug. 2017, pp. 118–123.

[48] B. Ganapathysubramanian and N. Zabaras, "Sparse grid collocation schemes for stochastic natural convection problems," *Journal of Computational Physics*, vol. 225, no. 1, pp. 652–685, 2007.

[49] X. Ma and N. Zabaras, "An adaptive hierarchical sparse grid collocation algorithm for the solution of stochastic differential equations," *Journal of Computational Physics*, vol. 228, no. 8, pp. 3084–3113, 2009.

[50] *ANSYS® Electronic Desktop, Release 17.2.*

[51] O. L. Maître, H. Najm, R. Ghanem, and O. Knio, "Multi-resolution analysis of wiener-type uncertainty propagation schemes," *Journal of Computational Physics*, vol. 197, no. 2, pp. 502 – 531, 2004. [Online]. Available: http://www.sciencedirect.com/science/article/pii/S0021999103006491

[52] M. Stoyanov, "User manual: Tasmanian sparse grids v4.0," Oak Ridge National Laboratory, Tech. Rep. ORNL/TM-2017/596, 2017.

[53] M. Gunzburger, C. G. Webster, and G. Zhang, "An adaptive wavelet stochastic collocation method for irregular solutions of partial differential equations," Oak Ridge National Laboratory, Tech. Rep. ORNL/TM-2012/186, 2012.

[54] M. Jansen and P. Oonincx, *Second Generation Wavelets and Applications*, New York: Springer, 2005.

[55] M. K. Stoyanov and C. G. Webster, "A dynamically adaptive sparse grids method for quasi-optimal interpolation of multidimensional functions," *Computers & Mathematics with Applications*, vol. 71, no. 11, pp. 2449–2465, 2016.